Floating algal beds and methane dynamics: a potential positive feedback loop

Sofia Baliña[1], José Paranaíba[1], Maite Colina[1], Stefan Weideveld[1], Sarian Kosten[1]

[1]Ecology Department, Radboud Institute for Biological and Environmental Sciences (RIBES), Radboud University, Nijmegen, the Netherlands

*Corresponding author: sofiabalinia@gmail.com

Email addresses, in the corresponding order: sofiabalinia@gmail.com, jose.paranaiba@ru.nl, maite.colinarama@ru.nl, stefan.weideveld@ru.nl, sarian.kosten@ru.nl

Peer review status: This is a non-peer-reviewed preprint submitted to EarthArXiv

Floating algal beds and methane dynamics: a potential positive feedback loop

Sofia Baliña[1], José Paranaíba[1], Maite Colina[1], Stefan Weideveld[1], Sarian Kosten[1]

[1]Ecology Department, Radboud Institute for Biological and Environmental Sciences (RIBES), Radboud University, Nijmegen, the Netherlands

Abstract

Eutrophic shallow freshwater ecosystems often develop floating filamentous microalgae on their surface during spring and summer, known as floating algal beds (FLAB). In recent years, FLAB has become more frequent and pronounced due to rising temperatures and drier conditions, sometimes even covering the entire surface of water bodies. New evidence suggests that phytoplankton can produce methane (CH_4) and it has also been reported that algal-derived carbon can enhance CH_4 production in the sediments, raising the possibility that FLAB may increase CH_4 emissions. However, FLAB may also reduce CH_4 emissions by decreasing CH_4 diffusion at the air-water interface and/or trapping CH_4 bubbles below the mat, thereby increasing the opportunity for microbial CH_4 oxidation before release to the atmosphere. Consequently, the net impact of FLAB on carbon emissions from freshwater ecosystems remains unclear. To address this knowledge gap, a field experiment consisting of a treatment covered with FLAB and a control (no FLAB) was carried out in a eutrophic shallow ditch. Diffusive and ebullitive CH_4 emissions increased by 12-fold and 5-fold, respectively, in the presence of FLAB, resulting in a 5-fold increase in CO_2-equivalent emissions. This increase appears to be linked to enhanced CH_4 production in the sediments fuelled by FLAB derived organic carbon, which was mostly relevant when anoxia developed beneath the mat. Overall, these findings indicate that FLAB blooms can substantially amplify carbon emissions from shallow aquatic ecosystems, with effects driven not only by FLAB biomass but also by mat-induced changes in water column dynamics and by intrinsic sediment properties.

Key words

Carbon emissions, ditches, ebullition, diffusion, sediment, freshwater ecosystems, eutrophication, oxidation, greenhouse gas

Highlights

- FLAB affected CH_4 and CO_2 fluxes from the ditch
- Total CO_2 equivalents were fivefold higher in the presence of FLAB
- FLAB effects depend on water column dynamics and sediment conditions

Introduction

Some species of filamentous freshwater algae can form floating clusters in wind-sheltered habitats (Hillebrand 1983). These clusters are often referred as metaphyton, pseudoplankton, pond scum or floating algal beds (FLAB) (Hillebrand 1983; Pikosz 2015; further used here). The initial development of these algae generally occurs at the sediment surface, where they survive through winter. After a period of submerged growth, they form tangled filamentous colonies that trap oxygen bubbles, which enables the colonies to rise to the surface where they continue to grow (Pikosz and Messyasz 2015; Mendoza-lera and others 2016; Pikosz and others 2017; Gladyshev and Gubelit 2019). This event typically occurs in spring to early summer, when increasing water temperatures, longer days, and higher radiation create key environmental conditions that promote floating algae development (Pikosz and Messyasz 2015; Gladyshev and Gubelit 2019). The rapid growth of FLAB is often followed by an equally rapid decay and decomposition phase when temperature and radiation decrease, where senescent masses sink or are washed ashore sometimes generating huge ecological and economic impacts (Gladyshev and Gubelit 2019). Floating mats can accumulate harmful concentrations of *Escherichia coli* (Whitman and others 2003) and disrupt ecosystem food webs (Page and others 2022), leading to negative consequences in the ecosystem. These effects taken together, alongside their wide distribution, contamination tolerance, occurrence in eutrophic habitats, and ease of identification, have led to the use of FLAB as indicators of deteriorating water quality (Whitton 1984; Philips 1990; Commission 2014; Gladyshev and Gubelit 2019). In addition, these dense floating algal mats shade the water column and may cause anoxia, inducing the death of deeper FLAB layers and of other organisms, ultimately reducing species diversity (Gladyshev and Gubelit 2019). They can also impact biogeochemical cycles through their impact on light availability, oxygen dynamics, organic matter accumulation, and nutrient cycling (Green and Fong 2016). While these ecological and biogeochemical impacts are considerably well documented, their consequences for the production, consumption, and emission of the major greenhouse gases methane (CH_4) and carbon dioxide (CO_2) remain poorly understood. As a result, the net effect of FLAB on aquatic greenhouse gas budgets is currently difficult to predict and therefore to include into ecological models.

Laboratory studies applying algal material directly onto sediment cores show that algae markedly increase CH_4 production (Uz and others 2007; Schwarz and others 2008; West and others 2012; Liang and others 2016), likely because algal carbon is more readily decomposed by methanogens than terrestrial carbon (West and others 2012; Grasset and others 2018). However, these experiments were all laboratory based, whereas in natural systems FLAB blooms develop at the water surface. As they age, deeper layers can decay, remain suspended, or accumulate in sediments, potentially influencing CH_4 dynamics throughout the whole water column. FLAB mats can affect

O_2 concentrations below the floating mat, which is a key driver of both CH_4 production and oxidation (Conrad 1999; Borrel and others 2011).They might also be able of producing CH_4, as shown for some phytoplankton taxa (Bižić and others 2020; Klintzsch and others 2020, 2023; Baliña and others 2025), suggesting that FLAB could be an overlooked source of CH_4. FLAB may also exert a physical effect by trapping CH_4 bubbles beneath the mat - as has been described for other types of floating vegetation (Attermeyer and others 2016; Kosten and others 2016) - diminishing ebullition and reducing the water-atmosphere gas exchange, thereby increasing CH_4 residence time and providing greater opportunity for microbial CH_4 oxidation before release to the atmosphere (Kosten and others 2016). At the same time, FLAB may also act as a strong daytime CO_2 sink, although this effect could be reversed at night (Peixoto and others 2016). Taken together, the net effect of FLAB on ecosystem carbon fluxes remains difficult to predict.

FLAB is usually favoured to grow in eutrophic and shallow systems with stagnant waters, limited wave and wind action (Pikosz and Messyasz 2015; Gladyshev and Gubelit 2019), such as drainage ditches. In the Netherlands, FLAB occurrence and proliferation in ditches during spring and summer - driven by inputs from agricultural wastewater and manure from surrounding pastures - were already reported more than forty years ago (Hillebrand 1983; Simons and Beem 1990; Simons 1994). Since then, continued eutrophication, higher irradiation in spring, rising temperatures, and increasingly dry, drought-prone conditions that promote stagnant water (KNMI 2026) have likely further intensified FLAB development, where they can sometimes even cover the entire surface of the ditch (Fig. S1). These climatic conditions are expected to promote even more frequent FLAB blooms in the future, yet their *in-situ* effects on CH_4 and CO_2 dynamics remain poorly understood, leading to an important knowledge gap in terms of total GHG emissions from eutrophic ditches. In this study, our main goals are: I) evaluate the effect of FLAB on the total GHG carbon emissions of a eutrophic ditch, by measuring CO_2 and CH_4 emissions in the presence and absence of FLAB; and II) identify the potential mechanisms driving changes in CH_4 emissions in the presence of FLAB. We hypothesize that: 1) both diffusive and ebullitive CH_4 emissions will increase in the presence of FLAB, whereas CO_2 emissions will decrease, changing the total ecosystem C-emissions; and 2) increased CH_4 emissions will be primarily driven by an extra input of algal organic matter in combination with anoxic conditions below the floating mat. To address these hypotheses, we carried out a five-day field experiment in a eutrophic Dutch ditch using eight open-bottom/open-top cylinders, four covered with FLAB and four left uncovered as controls. We directly measured or indirectly estimated all the CH_4-related processes: CH_4 diffusive and CH_4 ebullitive emissions, dissolved CH_4 concentrations and CO_2 diffusive emissions, were measured *in-situ* on a daily basis; incubations were carried out to estimate methane oxidation (MOX) rates, FLAB-related CH_4

production, and sediment CH_4 production. Emission measurements were used to evaluate potential changes in the total ecosystem C-emissions, whereas CH_4 mass balances were conducted for each replicate to investigate the potential drivers underlying FLAB effects on CH_4 dynamics.

Methods

1. Study site

Field experiments were carried out in a eutrophic drainaged ditch (51°55'18" N, 5°48'10" E) in the Netherlands, between 23rd and 30th August 2024. This region is used for intense agriculture with substantial agricultural runoff (RIVM 2024). The local climate is temperate marine, with temperatures ranges of 3 – 7°C in winter and 17 – 25°C in summer. The month August in the year 2024 was warm, with a mean temperature of 19.3°C (KNMI, 2024). The ditch was selected based on observed FLAB occurrences in previous years.

2. Field experiments

Experiments consisted of deploying eight enclosures made of transparent polycarbonate of 1mm thickness, with a size of 1m in height and 0.5m in diameter (maximum volume of 196 L and a surface area of 0.2 m^2) (Fig. S2). The lower 0.3 m of each enclosure was fitted with a stainless-steel rim to improve sediment grip and enhance overall stability (Fig. S2a, b). The surface and bottom of the enclosures were open to include all the relevant production and consumption CH_4 pathways associated with both sediment and water column processes, whereas lateral transport was inhibited by the walls. Four enclosures were covered with 4000g wet weight (WW; ~7 cm of height) of freshly collected FLAB (Fig. S2e) and four remained as a control, without FLAB. As no FLAB developed in the study ditch on August 2024, FLAB was collected from a nearby location (51°52'17.6" N, 5°51'04.9" E).

Inside all the enclosures an inverted plastic funnel attached to a glass bottle was placed, to collect gas bubbles. Also, in two treatment and two control replicates (randomly selected), and in the ditch (downstream the enclosures) oxygen and temperature high frequency sensors (MiniDOT, PME®) were placed 0.5m below the water surface (Fig. S2c), to posteriorly derive ecosystem metabolism rates. The enclosures were placed in the ditch on 23rd of August and left for 72hs to stabilize. Prior to installing the enclosures, sediment was inspected and any submerged macrophytes were removed. After placement, a fish net was used to ensure that the enclosures were fishless. On the 26th of August, FLAB was added, together with bubble traps and MiniDOTs. The measurements lasted until the 30th of August. To account for potential effects of the enclosures on CH_4 and CO_2

emissions, a set of four automatic chambers was also deployed directly in the ditch, downstream of the enclosures, from 26th to 30th August (Fig. S2d).

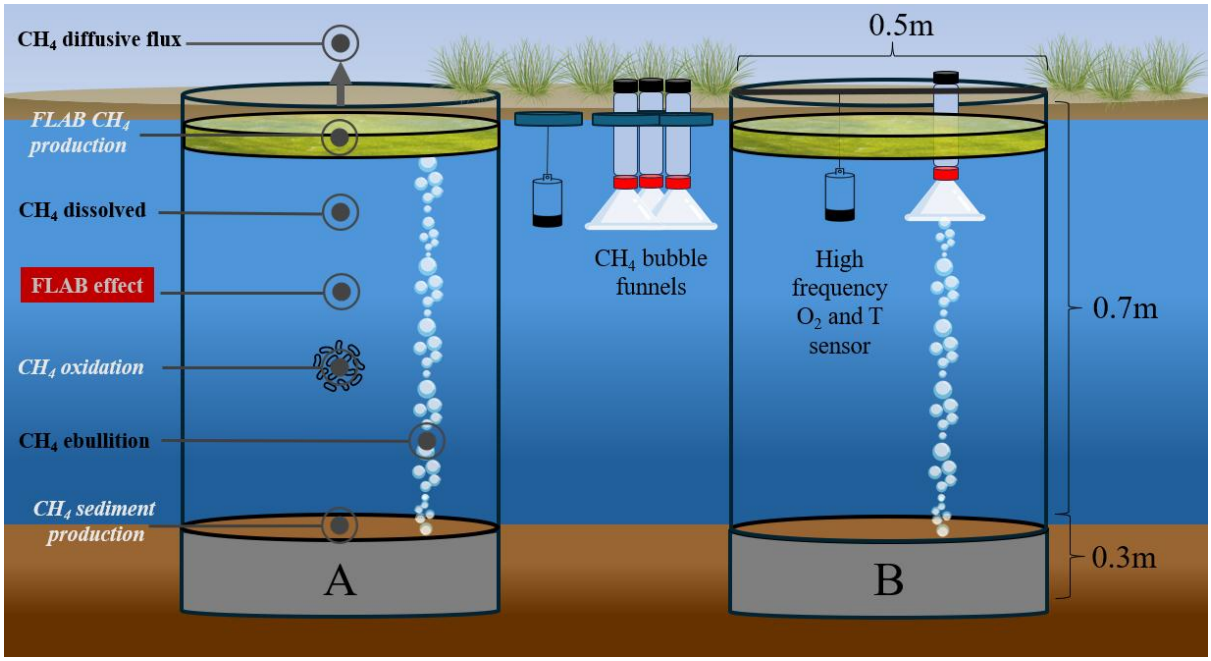

Figure 1. Schematic representation of the experimental design. A) Includes all the CH_4 related processes that were either directly measured (black and bold) or indirectly estimated (white and italics); B) includes dimensions of the enclosures, as well as the general setup, including the high frequency O_2 and T sensors (MiniDOT, PME®) and the bubble funnel; C) One MiniDOT and four bubble funnels were also placed in the ditch, attached to floating devices.

3. Limnological characterization

Remaining FLAB at the end of the experiment was collected from the surface of each replicate, its wet weight (WW) was recorded, and samples were dried at 70°C (Universal oven, Memmert, Germany) until constant weight, at which point the dry weight (DW) was determined. The WW:DW ratio obtained at the end of the experiment was applied to the initial WW to estimate the initial DW.

In addition to the high frequency sensors (MiniDOT, PME®), oxygen (O_2) and temperature (T) profiles were measured at 10 cm intervals (from just below the water surface until sediment) in each replicate and in two locations in the ditch (upstream and downstream of the enclosures), once per day every day. With the same frequency, subsurface (within the first 5cm) pH and conductivity were recorded for each enclosure and the ditch. All these measurements were taken using a portable multiparameter meter (HQ Series, Hach Company, Loveland, CO, USA) equipped with corresponding sensors (Hach, USA). On the 29th of August an irradiance profile was also carried out in one FLAB replicate, two control replicates and in the ditch. Photosynthetically active radiation (PAR, 400 – 700 nm) was measured using a LI-COR LI-250 Light Meter (LI-COR Biosciences, Lincoln, NE,

USA) coupled to a submersible quantum sensor US-SQS/L (WALZ Mess- und Regeltechnik, Effeltrich, Germany). Measurements were taken every 10cm from subsurface up to 50cm. The vertical light attenuation coefficient ($K_{d\ PAR}$) was estimated by fitting a linear regression between depth (m) and the natural logarithm of downwelling PAR irradiance (µmol photons m^{-2} s^{-1}), where the regression slope corresponds to $K_{d\ PAR}$ ($\ln I = K_{d\ PAR} \times \text{depth} + b$) (Kirk 2011). The euphotic depth, defined as the depth receiving 1% of surface PAR, was calculated by inserting ln (0.01 × surface irradiance) into this regression and solving for depth (Kirk 2011).

On the first and last day of the experiment subsurface water samples (within the first 10cm) were collected from each replicate and the ditch to carry out the following analyses: a) phosphate (PO_4^{3-}), nitrate (NO_3^-) and ammonium (NH_4^+) concentration (from 15ml of water preserved at -20°C), on a SEAL AA3 HR AutoAnalyzer (SEAL Analytical) using standard methods; b) total organic carbon (TOC) from unfiltered water and dissolved organic carbon (DOC) from water filtered through GF/F glass microfiber filters (1.2 µm pore size, 47 mm diameter; Cytiva Whatman, Maidstone, UK). In both cases, 10 ml samples were preserved with 0.1 ml 2M HCl solution at 4°C upon analysis, on a Analytik Jena multi-N/C 3100 analyzer; c) Chlorophyll a (Chla-a) from a known volume of water filtered through glass GF/C microfiber filters (1.2 µm pore size, 47 mm diameter; Cytiva Whatman, Maidstone, UK), posteriorly stored at -20°C. Upon analysis, Chl-a was extracted using 10ml of 95% cold ethanol and left overnight at 4°C and under dark conditions. After 24hs, the absorption in the wavelengths of 665 and 750 was measured before and after acidification with 0.12N HCl solution (ISO 10260, 1992).

4. Ecosystem metabolism

Ecosystem gross primary production (GPP), respiration (R) and net ecosystem production (NEP) rates were estimated by means of high-frequency oxygen and temperature data (miniDO$_2$T, Precision Measurement Engineering, Inc.®), following Soued and Prairie (2021). Ecosystem metabolism rates were calculated based on a diurnal open system O_2 model (Odum, 1956), where changes in O_2 concentration are a function of GPP, ER, and O_2 exchange at the water-air interface (KO_2), following equation 1.

$$\frac{dO_2}{dt} = \frac{GPP}{Z_{epi}} + \frac{ER}{Z_{epi}} + K_{O2}(O_{2\,sat} - O_2) \qquad equation\ 1$$

Were Z_{epi} is the epilimnion depth, which in our case is the mean depth of each enclosure or the ditch, respectively, for the entire duration of the deployment. $O_{2\,sat}$ is the theoretical concentration of O_2 at saturation, considering the in-situ temperature and atmospheric pressure. O_2 is an empirically measured oxygen concentration in the water. Detailed equations of the model can be found in Hall & Hotchkiss (2017).

Daily estimates of GPP and ER were obtained through maximum likelihood using equation 1 and the R package Stream Metabolizer (Appling and others 2018). Net daily primary production (NPP) was then calculated as GPP

- ER. A final mean value ± standard deviation of GPP, ER, and NPP was obtained for each replicate and the ditch for the entire duration of the experiment.

5. Greenhouse gas dynamics

5.1 CH_4 dissolved in the water

The concentration of CH_4 dissolved in the water was obtained by means of the headspace technique (Magen and others 2014). Approximately 6ml of water was injected into 12ml pre-vacuumed exetainers (Labco exetainer®) containing 0.1ml of H_2SO_4 1M as fixing solution and afterwards stored at room temperature. Upon analysis, the samples were flushed with pure N_2 to equilibrate pressures, vigorously shaken for 2 minutes to ensure mixing between the air and water phases, and posteriorly 100µl (by triplicate) analysed in a methane GC-FID (Shimadzu, Nexis, CG-2030) associated to an autosampler (Shimadzu, AOC-6000 Plus). Before every batch run, a calibration curve was made. CH_4 concentration in the sample was calculated according to Henry's law for the given temperature and salinity (Sander 2015).

In each of the eight replicates and in the two sites from the ditch (upstream and downstream of the enclosures), samples of dissolved CH_4 were taken once a day on the 26th (afternoon) and the 30th of August (morning), and twice a day (in the morning and afternoon) between the 27th and 29th, obtaining a total of eight samples for each enclosure as well as for the two points in the ditch. Each measurement had a methodological duplicate.

5.2 CH_4 and CO_2 fluxes

5.2.1. Air: water interface CH_4 and CO_2 fluxes from enclosures

CH_4 and CO_2 diffusive emissions (mg m^{-2} d^{-1}) from the enclosures were obtained by placing a lid on top of the enclosures, which was connected to an ultra-portable greenhouse gas analyzer (GGA, Los Gatos Research, ABB Inc., San Jose, CA, USA), creating a closed loop. The lid was made from transparent polycarbonate (0.6cm thick), had an extra sealing rim covering the external borders of the internal face to improve the sealing (1cm width), and a surface of 0.2m^2 (Fig. S3). Each measurement lasted three minutes and, since measurements were monitored in real time, any abrupt increase in CH_4 emissions during the three-minute deployment was considered as a CH_4 bubble intrusion, and the diffusive flux measurement was discarded and repeated. The height of the headspace of each enclosure was measured every day, to account for any potential differences water level. The diffusive fluxes were calculated based on robust linear models using the gasfluxes package (Fuss 2024) in R (R Core Team 2025), following equation 2, 3 and 4 (Zhao and others 2018).

$$F = \frac{10VP_0\left(1-\frac{W_0}{1000}\right)f_0}{RS\,(T_0+273.15)} \qquad equation\ 2$$

where V (cm^3) is the chamber volume, P_0 (kPa) is the initial air pressure, W_0 (mmol mol^{-1}) is the initial water vapor mole fraction, f_0 is the initial rate of change in water-corrected CO_2 or CH_4 mole fraction (µmol mol^{-1}) inside the chamber, R is the gas constant (8.314 Pa m^3 K^{-1} mol^{-1}) and T_0 (°C) is the initial air temperature. To estimate f_0 a linear regression algorithm was used, using the least squared method to fit a straight line (equation 3)

$$C = a_0 + a_1 t \qquad equation\ 3$$

Where a_0 and a_1 are the intercept and slope of the regression line, respectively, and t is the time. Considering this, f_0 can be calculated as

$$f_0 = \frac{\partial C}{\partial t} \int_{t=t0}^{\cdot} = a_1 \qquad equation\ 4$$

Average wind (m s^{-1}), atmospheric pressure (hPa) and atmospheric temperature (°C) were recorded in situ during diffusive flux measurements, using a hand-anemometer (Kestrel 3000 Pocket Weather Meter, Nielsen-Kellerman Co., Boothwyn, PA, USA). These diffusive fluxes were measured in total eight times in each enclosure, twice a day (in the morning and afternoon) between the 26th and 29th of August, and only in the morning on the 30th of August. Diffusive flux measurements were coupled to CH_4 dissolved sample retrieving, and they were all done during daytime.

5.2.2 Air: water interface CH_4 and CO_2 diffusive fluxes from the ditch

Downstream the enclosures, four floating, transparent, and automated cylinder-shaped chambers (height = 51 cm, inner diameter = 39 cm) were deployed (Fig. S2d). Each chamber was placed on top of a floating collar to ensure buoyancy and tied to both sides of the ditch to avoid drifting. Chambers had a transparent flat lid associated to a stepper motor, which was connected to a multiplexer with an integrated pump (2.5 L min^{-1}) (Nijman and others 2024). The multiplexer ensured that one chamber was closed at a time and facilitated gas circulation between the chambers and an ultra-portable greenhouse gas analyzer (GGA, Los Gatos Research, ABB Inc., San Jose, CA, USA). The CO_2 and CH_4 flux inside each chamber were measured for 3-min and followed by 30 seconds flushing time in between closures. A temperature logger (HOBO Pendant MX Temp, Onset Computer Corporation, Bourne, MA, USA) was placed inside each chamber, to continuously record air temperature. Total fluxes (mg m^{-2} d^{-1}) were calculated as described in section 5.2.1, following equations 2, 3 and 4. This automatic setup was powered by batteries, since there was no access to the electrical grid. This method of powering the system introduced problems that led to occasional interruptions in data logging.

Since CO_2 and CH_4 fluxes were recorded semi-continuously, these measurements include total fluxes: diffusive CH_4 emissions but potentially CH_4 ebullitive emissions too. Given that the latter were accounted for with bubble

funnels, these were not obtained from the semicontinuous data. All 628 measured fluxes were individually inspected for CH_4 bubble intromission and to assure linearity. From the whole data set, 32% had to be removed because it had either CH_4 bubble intromissions, not a linear CH_4 increase or started with a very high CH_4 baseline, the remaining 68% fulfilled the requirements needed to be compared with the diffusive fluxes from the enclosures.

5.2.3 CH_4 ebullitive emissions

CH_4 ebullitive emissions (mg m^{-2} d^{-1}) was estimated in each enclosure and in the ditch, by placing funnels with an area of 0.03 m^2 attached to inverted 350 ml glass bottles filled with water. One funnel was placed in each replicate (Fig. S4a), and four funnels attached to floaters were placed in the ditch (Fig. S4b), upstream the enclosures. When enough volume was accumulated, 3ml samples of the bubbles were retrieved using a needle connected to a 3ml syringe through their rubber stopper, placed in 3ml pre-vacuumed exetainers (Labco exetainer ®) and stored in room temperature until analysis. Upon analysis, 50µl of the sample (by triplicate) was injected in a GC-FID (model 5890A, Hewlett-Packard, Palo Alto, CA, USA) First, the concentration of CH_4 (mg CH_4 L^{-1}) in the sample was obtained, considering the volume of sample injected (50µl), the slope of the calibration curve (area standard * nmol CH_4 $standard^{-1}$) and the molar mas of CH_4 (16.04 g mol^{-1}). CH_4 ebullitive flux was obtained using equation 5.

$$CH_4\ ebullitive\ flux\ = \frac{CH_4\ concentration * Total\ volume\ collected}{Funnel\ area * Deployment\ time} \qquad equation\ 5$$

Where CH_4 ebullitive flux (mg m^{-2} d^{-1}) is obtained considering the concentration of CH_4 in the gas sample (mg L^{-1}), the total volume of sample collected (L) in the bubble trap, the area of the funnel (m^2) and the total deployment time (days).

5.2.4 Sediment: water interface CH_4 diffusive emissions

The diffusive CH_4 emissions from sediment cores (mg m^{-2} d^{-1}) were obtained by taking a core from the ditch using a 1.2m height and 0.6m diameter acrylic liner. After extraction, part of the water column was gently removed, the headspace height was measured, and the core was set to rest for approximately an hour. Upon measurement, a lid with two connectors was placed on top of the core and connected to the GGA, creating a closed loop. Cores were taken from the ditch, downstream and upstream of the enclosures, on the 23rd and 29th of August. This procedure was repeated on the 18th and 24th of October, to assess potential temporal variability. All the cores were taken within approximately 3 meters of total distance and close to the experimental setup area. No cores were extracted from the enclosures, to avoid resuspension of sediments and, therefore, affecting the treatments. The diffusive sediment CH_4 fluxes were calculated as described for the enclosures, following equation 2, 3 and 4 (Zhao and others 2018).

5.3. CH_4 standardize gas exchange velocity (K_{600} CH_4)

CH_4 dissolved concentrations and CH_4 diffusive emissions in the air: water interface from the ditch and the treatments, alongside the wind measurements, were used to calculate the standardized exchange velocity for each case and each day (K_{600} CH_4). A detailed description of this calculation can be found in Suppl. Inf. 1.

5.4 Total GHG emissions (as CO_2 equivalents)

Total GHG emissions were estimated by summing CH_4 diffusive and ebullitive emissions (converted to CO_2 equivalents) and CO_2 diffusive emissions. We used a global potential warming (GPW) of 27 in a 100-year horizon for CH_4 (Forster and others 2021).

Because CO_2 diffusive fluxes were measured only during daytime, a correction was applied to account for higher nighttime emissions. Based on published studies comparing daytime and nighttime CO_2 fluxes in open water (Liu and others 2016; Attermeyer and others 2021; Gómez-Gener and others 2021) and floating macrophyte stands (Peixoto and others 2016), mean correction factors of 0.45 ± 0.22 and 0.43 ± 0.13 were derived, respectively. Nighttime fluxes were estimated by multiplying the measured daytime fluxes by the appropriate correction factor, assuming that systems acting as daytime CO_2 sinks became nighttime sources. Mean daily CO_2 fluxes were then calculated from the combined daytime and estimated nighttime values.

For CH_4 ebullitive emissions, two adjustments were applied to calculate CO_2-equivalent emissions. First, the sampling frequency differed between the ditch and the treatment: bubble funnels in the ditch accumulated enough bubbles for sampling on three separate days, whereas those in the control and FLAB treatments were sampled twice. Although individual fluxes were standardized to deployment duration, the unequal number of samples could still bias comparisons. To minimize this bias, we calculated CO_2-equivalent emissions based on the total mass of CH_4 emitted during the experimental time, rather than on individual flux measurements. For each replicate, the mass of CH_4 collected in all ebullition samples was summed and normalized by area (mg m^{-2}). This represents the total CH_4 mass released over the entire monitoring period. We then divided this total mass by the total deployment time (in days) for that replicate - whether from the ditch or from the treatments. The resulting rate (mg CH_4 m^{-2} d^{-1}) was then converted into CO_2 equivalents. This approach provides a more consistent and comparable estimate because it accounts for differences in sampling frequency between replicates and the ditch. Second, ebullitive CH_4 emissions measured in the FLAB treatment represent bubbles captured beneath the floating algal mat, but not necessarily the amount that reached the atmosphere. Floating mats can trap bubbles, reducing the fraction that escapes. To account for this potential retention, we applied a correction factor derived from Kosten et al. (2016), who quantified bubble retention under various types and densities of floating vegetation. Although

their vegetation types differed from the FLAB mats used in this study, they offer the best available analogue in literature. They reported bubble retention between 10% and 40%, with higher retention associated with greater biomass. We therefore applied 10% and 40% retention factors to the median CO_2 equivalents derived from CH_4 ebullition from the FLAB system, to estimate the corresponding lower- and upper-bound potential emission scenarios.

6. Methane oxidation rates (MOX) in the water

To estimate methane oxidation rates (MOX) in the water, water from the ditch itself was taken on the 27th of August and incubated in a total of eight 120ml glass bottles. In each bottle, 20ml of ditch water was placed, leaving a headspace of 100ml, 1 ml of pure CH_4 was added (1% of the headspace's volume) and bottles were sealed with rubber stoppers and aluminium crimp caps using a manual crimper, to ensure airtight conditions (Nijman and others 2022). Water was incubated under complete dark or complete light conditions, and there were four replicates per treatment. The incubations bottles were placed on an orbital shaker (GIO Gyrotory® Shaker, New Brunswick Scientific Co., Inc., Edison, NJ, USA), at 150 r.pm, to ensure continuous mixing of the water and headspace phases, in a room at 21°C. The concentration of CH_4 in the headspace of the bottles was measured every day for 5 days, by injecting a 100µl sample (by triplicate) of the headspace of each bottle in a GC-FID (model 5890A, Hewlett-Packard, Palo Alto, CA, USA). The µmol of CH_4 in the headspace were calculated considering the area of the peak, the slope of the calibration curve and the volume (ml) of the headspace in the bottle. Afterwards, the nmol of CH_4 dissolved in the water phase were obtained following equation 6.

$$CH_4 dissolved = \frac{CH_4 headspace * CH_4 solubility}{\frac{water\ volume}{headspace\ volume}} \qquad equation\ 6$$

Where CH_4 dissolved (nmol) corresponds to the CH_4 dissolved in the water, CH_4 in the headspace (nmol) is the mass of CH_4 in the headspace phase, CH_4 solubility is obtained as $CH_4 solubility = Kh * RT, where\ Kh\ for\ 293K\ and\ 1atm\ pressure\ is\ 0.0015\ M/atm$, and water volume (ml) divided by headspace volume (ml) corresponds to the ratio between the headspace and water phases. The final concentration of CH_4 in µmol L^{-1} was obtained by relativizing for the water volume (L) in each incubation bottle, and by converting nmol to µmol. From these incubations, a regression between CH_4 dissolved (µmol L^{-1}) and time (days) was obtained, where the slope corresponds to the CH_4 oxidation (MOX) rate (µmol L^{-1} day^{-1}).

7. FLAB-related CH_4 production

To evaluate the potential for FLAB- related CH_4 production, 120ml glass bottles containing either only 20ml of ditch water (control) or 20ml of ditch water + 0.5gr of FLAB wet weight (treatment), in both cases leaving a 100ml headspace, were incubated under different temperature and CH_4 concentration conditions: 1) light and no

extra CH_4 addition; 2) light and 1ml of CH_4 added; 3) dark and no extra CH_4 addition; 4) dark and 1ml of CH_4 added. Bottles were sealed with rubber stoppers and aluminium crimp caps, to ensure airtight conditions. Incubation bottles were placed in a room with a controlled temperature of 21°C and on an orbital shaker (GIO Gyrotory® Shaker, New Brunswick Scientific Co., Inc., Edison, NJ, USA), at 150 r.pm, The concentration of CH_4 in the headspace of the bottles was measured every day for 5 days, by injecting a 100µl sample of the headspace of each bottle in a GC-FID (model 5890A, Hewlett-Packard, Palo Alto, CA, USA) with manual injection. Alongside the samples, a calibration curve was also run. The µmol of CH_4 in the headspace were calculated considering the area of the peak, the slope of the calibration curve and the volume (ml) of the headspace in the bottle. Afterwards, the nmol of CH_4 dissolved in the water phase were obtained following equation 6. The final concentration of CH_4 in µmol L^{-1} was obtained by relativizing for the water volume (L) in each incubation bottle. To ensure the incubation bottles did not become anoxic, O_2 concentrations in all the bottles were measured at the end of the incubation period using a Microx TX3 oxygen microsensor (flat-broken needle tip, Presens, Germany).

8. Sediment incubations to assess sediment CH_4 production and oxidation.

On the final day of the experiment (30th of August), three different 120cm core liners were used to extract one core from the ditch, one core from one of the control replicates and one from the FLAB replicates, the last two randomly selected. Back in the laboratory, each core was sliced to prepare incubations to estimate sediment CH_4 production (PROD) and CH_4 oxidation (MOX) rates. From each core, the first 2cm were incubated to estimate MOX rates, whereas the second following 4cm were incubated to estimate PROD rates, following Nijman and others 2022 and Struik and others 2024. For MOX rates, approximately 5g of wet sediment weight were placed in 120ml glass bottles with 15ml of water coming from that same system, and five replicates per core were created. Each bottle was sealed with rubber septa and aluminium crimp caps using a manual crimper to ensure airtight conditions. After sealing, a volume corresponding 10% of the headspace of the bottle (1ml) of pure CH_4 was injected to each bottle. Methane concentration in the headspace of each bottle was measured twice a day for five days. For PROD rates, approximately 25g of wet sediment wet weight was placed in a 120ml glass bottle with 15ml of water coming from that same system (previously flushed with pure N_2 to remove O_2), also creating five replicates per core. The preparation of PROD incubations was done in an anoxic chamber to ensure anoxic conditions. Methane concentration in the headspace of each bottle was measured once a day for five days. All MOX and PROD bottles were placed in an orbital shaker (GIO Gyrotory® Shaker, New Brunswick Scientific Co., Inc., Edison, NJ, USA), at 150 r.pm, in a room with controlled temperature of 21°C and under complete dark conditions. The concentration of CH_4 in the headspace of each bottle was measured using a GC-FID (model

5890A, Hewlett-Packard, Palo Alto, CA, USA) with manual injection. The nmol of CH_4 in the headspace were calculated considering the area of the peak, the slope of the calibration curve and the volume (ml) of the headspace in the bottle. Afterwards, the nmol of CH_4 dissolved in the water phase were obtained following equation 6. Once the incubations were over, all the incubation bottles were opened and placed in a 70°C drying oven (Binder GmbH, Tuttlingen, Germany) until constant weight. Sediment dry weight was recorded for each replicate and finally rates of CH_4 production as nmol day^{-1} g dry or wet $weight^{-1}$ were obtained.

9. CH_4 mass balance in the enclosures

To assess the effect of FLAB on ditch CH_4 dynamics, CH_4 mass balances were carried out for each replicate. Because the side walls of the enclosures substantially reduced lateral transport (Suppl. Inf. 2), lateral inputs were considered negligible and were therefore excluded from the mass balance. Also, since this ecosystem is very shallow (less than one meter depth), CH_4 bubble dissolution in the water column was considered as negligible (Joyce and Jewell 2003; McGinnis et al. 2006). Consequently, the change in CH_4 dissolved in the enclosures (ΔCH_4) would be the result of the sum up of sediment flux (Sed) plus the effect of FLAB ($FLAB$, below explained in detail), minus CH_4 oxidation in the water column (MOX), and CH_4 diffusion to the atmosphere DIF), following equation 7.

$$\Delta CH_4 = Sed + FLAB - (MOX + DIF) \qquad equation\ 7$$

The effect of FLAB accounts for different potential processes: CH_4 production directly by FLAB, changes in MOX rates below the floating mat due to changes in CH_4 and O_2 concentration, enhancement of CH_4 production in the sediments due to FLAB decomposition (leading either to higher CH_4 diffussive emissions, but also potentially enhancing CH_4 bubble formation and, due to the presence of the FLAB mat, potentially bubble accumulation below the mat) in combinations with decreased O_2 concentration below the FLAB mat, that might furthermore favour CH_4 production. A schematic description of all effects can be found in Fig. S5.

Some of the components of the mass balance (equation 7) were measured directly *in situ* (such as ΔCH_4 and DIF, explained in sections 5.1 and 5.2.1, respectively) whereas others were estimated indirectly (Sed, $FLAB$, and MOX). Below, a description of how each one of these indirect processes were estimated is explained. In Table 1 the parameters used for each one of the estimations are detailed.

9.1. *Sed*: modelling sediment CH_4 production

Sediment CH_4 production rates (*Sed*) were measured through flux measurements from extracted cores (section 5.2.4) and by sediment incubations (section 8). Two different methods were used to have a more reliable and accurate estimation of the potential sediment CH_4 production rates. For the mass balance, a set of three potential

sediment production rates where used, and the best fit was selected. Also, *Sed* was corrected for the temperature in the sediments (which was measured *in situ* every day, in each enclosure) following equation 8 (Segers 1998).

$$P_{sedT} = P_{sed} * Q_{10\,sed}^{\frac{(T_{sed} - T_{ref})}{10}} \qquad equation\ 8$$

Where P_{sedT} refers to the production of CH_4 in the sediments corrected by the temperature normalized by the area of the enclosure (µmol day^{-1}), P_{sed} is the non-corrected CH_4 production in the sediments (µmol day^{-1}), $Q_{10\,sed}$ was considered 3 (Table 1), T_{sed} is the temperature in the sediments (°C) and T_{ref} was considered 20°C (Table 1).

9.2. MOX: modelling methane oxidation (MOX) rates in the water

The methane oxidation rate (MOX, µmol L^{-1} day^{-1}) was obtained as described in section 6. To estimate the mass of CH_4 oxidized at each time point, MOX was corrected for the temperature in the water following equation 9 (Segers 1998; Thottathil and others 2019).

$$MOX_T = MOX * Q_{10\,mox}^{\frac{(T_{water} - T_{ref})}{10}} \qquad equation\ 9$$

Where MOX_T is the temperature corrected MOX rate (µmol L^{-1} day^{-1}), MOX is the MOX rate obtained from the incubations (µmol L^{-1} day^{-1}), $Q_{10\,mox}$ was considered 2 (Table 1), T_{water} is the subsurface water temperature in the enclosures (°C) and T_{ref} is the reference temperature (20°C) (Table 1).

Because aerobic MOX depends on the availability of both O_2 and CH_4, either substrate may become limiting. Therefore, the MOX rate was additionally corrected using a dual-substrate Monod formulation, following equation 10 (Segers 1998; Martinez-Cruz and others 2015).

$$MOX_{corr} = MOX_T * \frac{(CH_4)}{(KCH_4 + CH_4)} * \frac{(O_2)}{(KO_2 + O_2)} \qquad equation\ 10$$

Where MOX_{corr} is the MOX rate corrected by O_2 concentration, CH_4 concentration and temperature (µmol L^{-1} day^{-1}), MOX_T is the temperature corrected instantaneous MOX rate (day^{-1}) obtained from equation 9, CH_4 is the concentration (µmol L^{-1}) at each time point, KCH_4 is the half saturation constant of CH_4 for MOX (µmol L^{-1}, Table 1), O_2 is the subsurface O_2 concentration in the enclosure at each time point (mg L^{-1}) and KO_2 is the half saturation constant of O_2 for MOX (mg L^{-1}, Table 1).

9.3 *FLAB*: modelling FLAB effect as CH_4 production from a pool of decayed organic matter

The potential for CH_4 production induced by FLAB was estimated through laboratory incubations, and the indirect effect that the floating may exert on MOX rates by changing O_2 and CH_4 concentrations below the mat are also considered within the MOX corrections explained in section 9.2. Therefore, in the mass-balance model the FLAB component was considered as an additional source of CH_4 production in the sediments due to decomposition of

the organic carbon (OC) in the decayed pool of FLAB. The consumption of OC was modelled following equation 11 (Westrich and Berner 1984; Adair and others 2010; Forney and Rothman 2012).

$$\frac{dOC}{dt} = I - k * OC(t) \qquad equation\ 11$$

Where $\frac{dOC}{dt}$ is the change in the organic carbon (OC) pool in time, I is the input rate of OC (gr day^{-1}), k is the decay constant for OC decomposition coming from phytoplankton (day^{-1}) and $OC(t)$ is the organic carbon (g) at a certain time point.

This equation can be derived, and the solution is equation 12.

$$OC(t) = \frac{I}{k}\ (1 - \ e^{-kt}) \qquad equation\ 12$$

The input rate of OC (I, gr day^{-1}) refers to the amount of organic carbon transferred to the sediments per unit of time. To calculate this rate, we first determined the total dry-weight loss of FLAB over the experimental period by subtracting the final dry weight from the initial dry weight. The corresponding organic carbon (OC) content was then estimated as 44.8% of the total dry-weight loss, following Grasset et al. (2018). This total OC loss (g) was divided by 48 hours (the period during which FLAB production peaks) to obtain the input rate expressed in g day^{-1}.

After this, the OC obtained from equation 12 was converted to CH_4 production, following equation 13 (Segers 1998).

$$CH_4\ rate\ (t) = f * k * OC\ (t) \qquad equation\ 13$$

Where $CH_4\ rate\ (t)$ is the CH_4 production rate due to OC decomposition at a certain time point (gr day^{-1}), f is the fraction of OC that is converted to CH_4 (unitless), k is the decay constant of OC coming from phytoplankton (day^{-1}) and $OC\ (t)$ is the modelled OC (gr) at a certain time point, obtained from equation 12.

Table 1. Parameters used to model each one of the indirectly derived components of the mass balance.

Mass balance considerations		
Component	**Parameter**	**Reference**
Sed	$Q_{10\ SED}$ = 3 T_{ref} (°C) = 20	Segers 1998; Liikanen and others 2002; Duc and others 2010
FLAB	OC content in phytoplankton = 44.8 % k (day^{-1}) = 0.034 f (unitless) = 0.01 – 0.04	Grasset and others 2018 Grasset and others 2018 Segers 1998
MOX	$Q_{10\ MOX}$ = 2 K_{O2} (mg L^{-1}) = 0.25 K_{CH4} (µmol L^{-1}) = 3	Segers 1998; Thottathil and others 2019 Guérin and others 2007 Segers 1998

The final mass balance used to model CH_4 concentrations in each replicate is detailed in equation 14.

$$CH_t = \ CH_{4\,t-1} + dt * \big(Sed + FLAB - (MOX + DIF)\big) \qquad equation\ 14$$

Where $CH_{4\,new}$ (µmol) is the modelled mass of CH_4 concentration at each time point, $CH_{4\,t-1}$ (µmol) is the CH_4 mass at the previous time (the model was initiated with the CH_4 mass in each replicate at the onset of the experiment), dt is de delta time within each sampling point (day^{-1}), Sed is the corrected and surface scaled sediment CH_4 production rate (µmol day^{-1}), $FLAB$ is the volume scaled CH_4 production rate coming from FLAB decomposition (µmol day^{-1}), MOX is the corrected and volume scaled CH_4 oxidation rate (µmol day^{-1}) and DIF is the surface scaled CH_4 diffusive flux (µmol day^{-1}). It is important to notice that the *Sed* and *DIF* are surface related processes, whereas *MOX* and $FLAB$ are volumetric related processes, so each one of these rates were scaled to the area and volume, respectively, of each replicate at each time point. The surface of each replicate did not change throughout the experimental period, but the total volume inside each replicate had small changes that were considered in the calculations. Once the mass balance is done, the obtained $CH_{4\,new}$ mass at each time point can be converted to concentration by scaling it to the volume of each replicate at each time point, and this is depicted in Fig. 6 and Fig. S15. This modelled CH_4 concentration can be compared to the observed dissolved CH_4 concentration in each replicate at each time point, to check if the predictive concentration fits the observed one.

10. Statistical analysis

All statistical analyses were performed in R (version 4.4.1; R Core Team 2025). Dissolved CH_4 concentrations were modelled using a generalized linear mixed-effects model (GLMM) with a Gamma distribution and a log link function, implemented in the glmmTMB package (Brooks and others 2017). Replicate ID was included as a random effect to account for repeated measurements over time. Given the large differences in variance among treatments, the model included a variance structure dependent on Treatment (dispformula = ~ Treatment) to improve model fit. Model diagnostics were evaluated using simulated residuals from the DHARMa package (Hartig 2023), including checks for uniformity and overdispersion, which indicated that the model adequately captured the data. Post-hoc pairwise comparisons of treatments within each sampling day were performed using estimated marginal means from the emmeans package (Lenth 2023), with Sidak adjustment for multiple comparisons, and compact letter displays were generated to summarize significant differences among treatments for each day.

Results

1. Limnological parameters

When including data for the whole experimental period, pH, conductivity, phosphate and ammonium were similar among the ditch, the control and FLAB replicates (Table 2). Parameters related to water turbidity, such as secchi depth, $K_{d\,PAR}$, ash free dry weight (AFDW), dissolved organic carbon (DOC) and total organic carbon (TOC) were

similar between the ditch and the control treatment, but they were considerably higher in the FLAB treatment (Table 2). Similarly, CH_4 subsurface dissolved concentrations were higher in FLAB treatment, but similar between the ditch and the control treatment. Nitrate was similar between the control and FLAB treatment, but it was considerably higher in the ditch. The ecosystem metabolism based on diel O_2 fluctuations indicated an overall autotrophic metabolism for the ditch, a near-neutral metabolism for the control treatment and heterotrophic metabolism for the FLAB treatment. Note that we may miss autotrophic activity in the FLAB treatment as FLAB produced O_2 may have been emitted directly to the atmosphere and is not detected by the O_2 probes. When differentiating between beginning and end of the experimental period, the biogeochemistry in the ditch and control treatments changed little over time. In contrast, the FLAB treatment exhibited a clear shift, with higher dissolved CH_4 and elevated DOC concentrations at the end (Fig. S6).

The day-time temperature profiles for the ditch and the enclosures (Fig. S7) showed a consistent pattern across all treatments, with a well-mixed water column and similar temperature ranges. In contrast, day-time dissolved O_2 profiles (Fig. S8) exhibited treatment-specific dynamics. All systems began the experiment with similarly high O_2 subsurface concentrations, which declined over time but following different patterns. In the ditch, dissolved subsurface O_2 decreased from 13.3 ± 0.0 mg L^{-1} to 3.0 ± 0.1 mg L^{-1} by the end of the experiment. The control treatment showed a smaller decline, from 16.4 ± 0.9 mg L^{-1} to 9.8 ± 0.3 mg L^{-1}. In the FLAB treatment, enclosures started at 15.3 ± 1.5 mg L^{-1}, but three (#1, #5, and #6) became nearly anoxic by the end (0.8 ± 0.4 mg L^{-1}), whereas #8 still had a concentration of 7.2 ± 0.1 mg L^{-1} on the final day.

Table 2. Limnological parameters for the ditch, the enclosures control and the enclosures with FLAB. Values represent the mean for the experimental period ± standard deviation.

Parameter	Ditch	Control	FLAB
Secchi depth (m)	0.6 ± 0.1	0.6 ± 0.0	-
$K_{d\,PAR}$ (m^{-1})	5.0 ± NA	6.9 ± 5.3	35.4 ± NA
Euphotic depth (m)	0.9 ± NA	1.7 ± 1.3	0.2 ± NA
Water T (°C)	20.3 ± 0.1	20.6 ± 0.1	21.1 ± 0.3
pH	7.6 ± 0.0	7.9 ± 0.1	7.9 ± 0.2
Conductivity (µS cm^{-1})	585.8 ± 0.8	532.8 ± 4.1	532.9 ± 14.0
Dissolved O_2 (mg L^{-1})	6.9 ± 0.1	11.7 ± 0.7	10.1 ± 1.5
Dissolved CH_4 (µmol L^{-1})	1.5 ± 0.3	0.8 ± 0.5	11.0 ± 14.0
AFDW (mg L^{-1})	7.7 ± 1.9	9.4 ± 2.7	18.7 ± 6.6
DOC (mg L^{-1})	4.7 ± 1.3	4.5 ± 0.7	9.6 ± 3.5
TOC (mg L^{-1})	3.9 ± 1.1	5.7 ± 1.0	20.6 ± 14.9
PO_4^{3-} (µmol L^{-1})	0.1 ± 0.0	0.3 ± 0.8	0.2 ± 0.2
NO_3^- (µmol L^{-1})	9.3 ± 5.9	1.7 ± 3.0	3.3 ± 3.7
NH_4^+ (µmol L^{-1})	2.5 ± 0.8	1.9 ± 0.6	2.1 ± 0.6
Chla (µg L^{-1})	42.5 ± 17.0	20.7 ± 3.4	45.5 ± 30.2
GPP (g O_2 m^{-2} d^{-1})	20.7 ± 3.3	1.7 ± 0.1	4.5 ± 1.2
RE (g O_2 m^{-2} d^{-1})	-18.0 ± 2.9	-2.0 ± 0.1	-5.9 ± 1.0
NEP (g O_2 m^{-2} d^{-1})	2.7 ± 0.6	-0.3 ± 0.0	-1.4 ± 0.2

$K_{d\ par}$ (attenuation coefficient for photosynthetically active radiation); AFDW (ash free dry weight); DOC (dissolved organic carbon); TOC (total organic carbon); PO_4^{3-} (phosphate); NO_3^- (nitrate), NH_4^+ (ammonium); Chla (Chlorophyll a). All measurements correspond to subsurface samples (within the first 10cm of the water column).

2. Greenhouse gas (CH_4 and CO_2) dynamics

The pattern of dissolved CH_4 concentrations was similar between the ditch and the control treatment but differed for the FLAB treatment. From 28th of August onward, CH_4 concentrations in the FLAB treatment increased markedly and continued to rise until the end of the experiment, reaching a final mean value of 28.9 ± 16.6 µM, considerably higher than the final concentration in the ditch (1.4 ± 0.4 µM) and in the control treatment (1.7 ± 0.3 µM). The large standard deviation in CH_4 concentrations within the FLAB treatment reflects substantial variability among replicates, driven primarily by one of them (enclosure #8), which consistently exhibited lower CH_4 concentrations than the other FLAB replicates, but that remained higher than those in the control treatment and the ditch.

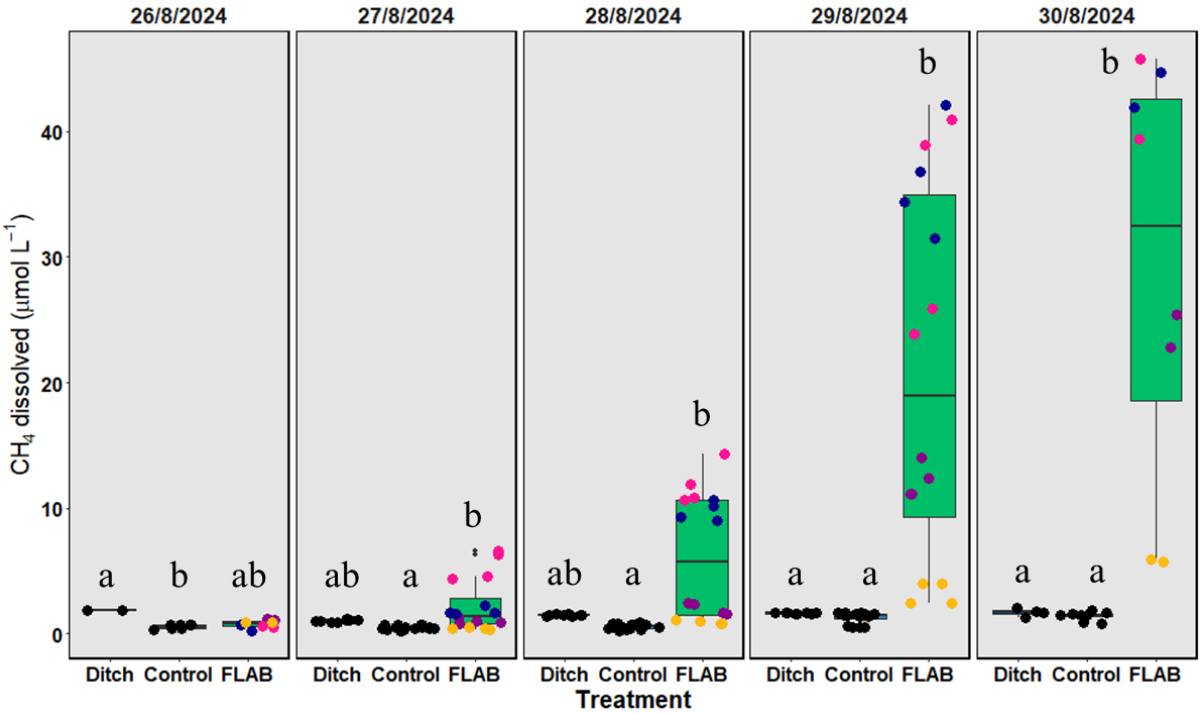

Figure 2. Methane (CH_4) dissolved concentration (µmol L^{-1}) in the ditch, the control treatment and the FLAB treatment. Panels indicate the sampling dates throughout the experimental period. Each point corresponds to the dissolved CH_4 concentration *per* sample and two samples were taken *per* replicate and *per* day, which was accounted for in the statistical analysis. All measurements were done during daytime. Different letters indicate statistically significant differences between treatments from the same date. Colours in the FLAB treatment indicate individual replicates: #1 (purple), #5 (pink), #6 (blue), and #8 (yellow).

Diffusive CH_4 emissions (Fig. 3) followed a similar pattern as CH_4 dissolved concentrations. For the ditch, data was collected on the 26th, 27th and 29th of August, with mean overall value for the whole experimental period of 0.1 ± 0.2 mg m^{-2} d^{-1} (Fig. S9). The control treatment had higher CH_4 diffusive emissions than the ditch, ranging between 0.8 ± 0.3 and 4.1 ± 1.5 mg m^{-2} d^{-1} at the beginning and the end of the experiment, respectively. The FLAB treatment exhibited a strong increase in CH_4 diffusive emissions through the experiment, with emissions starting at 3.5 ± 3.3 and ending at 78.4 ± 44.5 mg m^{-2} d^{-1}. The large standard deviation in the flux at the end of the experimental period reflects substantial variability among FLAB replicates, again driven primarily by replicate #8, which exhibited very low diffusive flux (2.9 ± 0.1 mg m^{-2} d^{-1}) in comparison with the rest of the FLAB replicates (97.3 ± 14.1 mg m^{-2} d^{-1}). The control and FLAB treatments exhibited daily K_{600} CH_4 within the same range (Fig. S10), indicating that the differences in diffusive emissions are related to the treatment itself and not to differences in physical conditions. The lower CH_4 diffusive flux for the ditch in comparison to the control treatment despite their similar CH_4 dissolved concentrations (Fig. 2) could be related to lower K_{600} CH_4 in the automatic chambers measurements (Fig. S10) as a result of lower turbulence due to their height and floating holders.

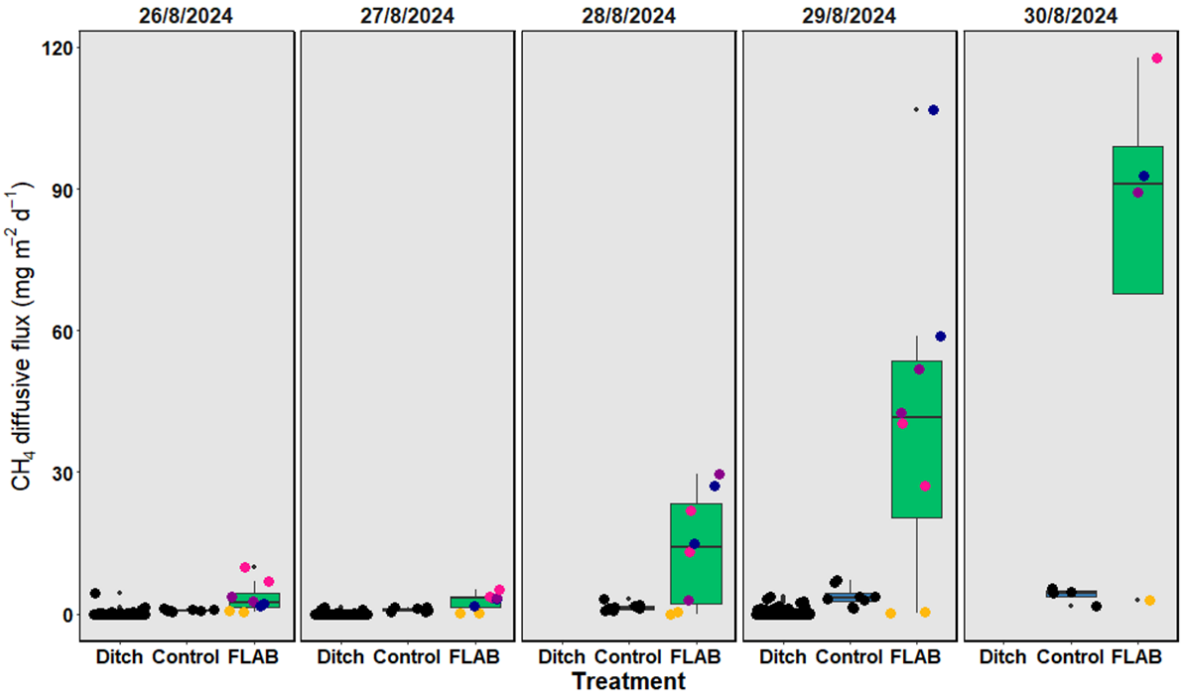

Figure 3. Methane (CH_4) diffusive flux (mg m^{-2} d^{-1}) from the ditch, the control treatment and the treatment with FLAB. Panels indicate the sampling dates throughout the experimental period. Each data point from the control and FLAB treatment corresponds to a flux measured: between the 26th and the 29th two measurements were done *per* day and *per* replicate (morning and afternoon), whereas on the 30th one measurement was done *per* replicate (morning). All measurements were done during daytime. Each data point for the ditch corresponds to the

automatically measured diffusive fluxes in the morning and/or afternoon of that day. Colours in the FLAB treatment indicate individual replicates: #1 (purple), #5 (pink), #6 (blue), and #8 (yellow).

Carbon dioxide (CO_2) diffusive flux (Fig. S11) had a very different pattern depending on the treatment. The ditch had similar fluxes during the three dates that data could be collected, and the mean overall value indicates that it was almost in equilibrium with the atmosphere, or a slight source (0.8 ± 0.7 mg m^{-2} d^{-1}) (Fig. S12). The control treatment started acting as a sink of CO_2 on the first day of the experimental period (-83 ± 76.6 mg m^{-2} d^{-1}) but then shifted towards being a net source of CO_2, with a mean flux of 306.0 ± 52.2 mg m^{-2} d^{-1} on the last day of the experiment. The FLAB treatment acted always as a substantial sink of CO_2, with an overall mean value of -1358.1 ± 417.5 mg m^{-2} d^{-1}. It is important to highlight that all these measurements were carried out during daytime, but these patterns will change and might even be reversed during nighttime.

Ebullitive CH_4 emissions had also a different pattern depending on the treatment and the moment of the experimental period (Fig. 4). In the ditch, there was enough trapped gas volume to retrieve samples at three different time points (28th, 29th and 30th of August) and from all four bubble funnels each time. Both the control and FLAB treatments produced enough bubble volume to allow sampling on two dates (28th and 30th August). Nearly all control and FLAB funnels yielded sufficient volume for both collections, except for replicate #8 from FLAB treatment, which accumulated enough bubbles only by the final sampling date (30th August) and this single sample corresponded to the lowest CH_4 ebullitive emission observed in the FLAB treatment (3.3 mg m^{-2} d^{-1}). Ebullitive emissions from the ditch (45.5 ± 32.3; 120.7 ± 83.8 and 82.8 ± 32.9 mg m^{-2} d^{-1} for the 28th, 29th and 30th, respectively) were of the same order of magnitude as those in the control treatment (33.8 ± 20.2 and 121.0 ± 148.8 mg m^{-2} d^{-1} for the 28th and 30th, respectively) and as those from the FLAB treatment on the 28th August sample retrieval (52.0 ± 41.4 mg m^{-2} d^{-1}) but emissions were higher for the FLAB treatment on the 30th August sample retrieval (539.1 ± 550.8 mg m^{-2} d^{-1}). The first bubble collection in the FLAB treatment reflects emissions produced within the first 48hs of experiment (from 26th to 28th August) and it was comparable in magnitude to the ditch and control treatment. The last bubble collection represents emissions produced in the last 48hs (29th and 30th of August), which were an order of magnitude higher and exhibited substantial variation among replicates, mainly driven by the low ebullitive emissions from replicate #8, following the same pattern observed for CH_4 dissolved concentrations (Fig. 2) and CH_4 diffusive emissions (Fig. 3).

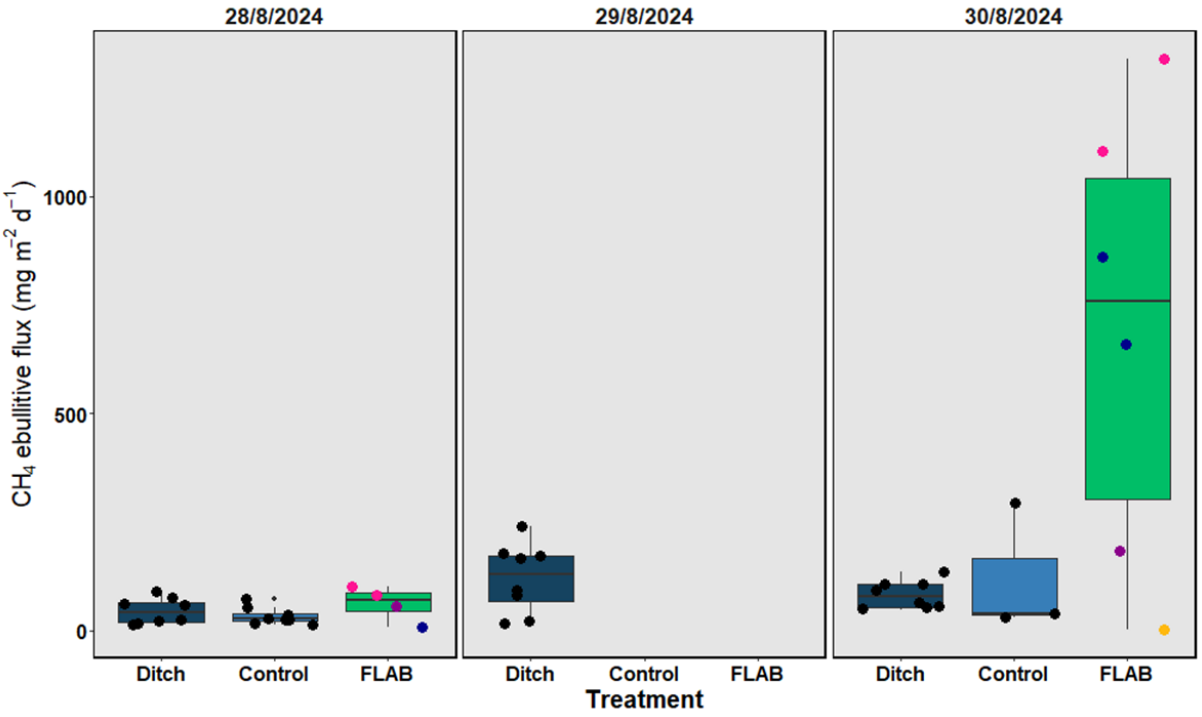

Figure 4. Methane (CH_4) ebullitive emissions (mg m^{-2} d^{-1}) from the ditch (dark blue), the control treatment (light blue) and the treatment with FLAB (green). Panels indicate the dates where there was enough gas collected to retrieve samples. In the ditch, samples could be retrieved from the four bubble funnels in three different time points (28th, 29th and 30th August), whereas in the control and FLAB treatments there was enough gas accumulated to retrieve samples in two different time points (28th and 30th August). On the 28th samples could be retrieved from three of the four FLAB replicates (not enough sample in replicate #8), but from all four control replicates. On the 30th samples could be collected from the four FLAB replicates, but from three of the four control replicates (not enough sample in replicate #2). Colours in the FLAB treatment indicate individual replicates: #1 (purple), #5 (pink), #6 (blue), and #8 (yellow).

CH_4 and CO_2 diffusive emissions alongside CH_4 ebullitive emissions were converted to CO_2 equivalents for the ditch, the control and the FLAB treatment, separately, following the considerations indicated in section 5.4 (Fig. 5). In all cases, the systems acted as net sources and the highest share corresponded to CH_4 ebullitive emissions. The ditch (2.0 ± 1.0 g CO_{2eq} m^{-2} d^{-1}) and the control treatment (1.8 ± 1.8 g CO_{2eq} m^{-2} d^{-1}) yielded overall similar mean CO_2 equivalent emissions. In contrast, the treatment with FLAB yielded considerably higher and much more variable mean CO_2 equivalent emissions (8.2 ± 8.0 g CO_{2eq} m^{-2} d^{-1}). This high variation is related to the variability among FLAB replicates, driven mostly by one of the four replicates (#8). Only for the CH_4 ebullitive pathway from the FLAB treatment a consideration of potential CH_4 bubble retention between 10% and 40% below the FLAB mat was applied, obtaining a new median value in each case (Fig. 5). If there was no bubble retention at all, the median value would be 6.7 g CO_{2eq} m^{-2} d^{-1} (black line), whereas with a 40% retention (more probable at the beginning of the experimental time) the new median would be 4.2 g CO_{2eq} m^{-2} d^{-1} (red dashed line) and with

a 10% retention (more probable at the end of the experimental time) the median would be 6.3 g CO_{2eq} m^{-2} d^{-1} (yellow dashed line).

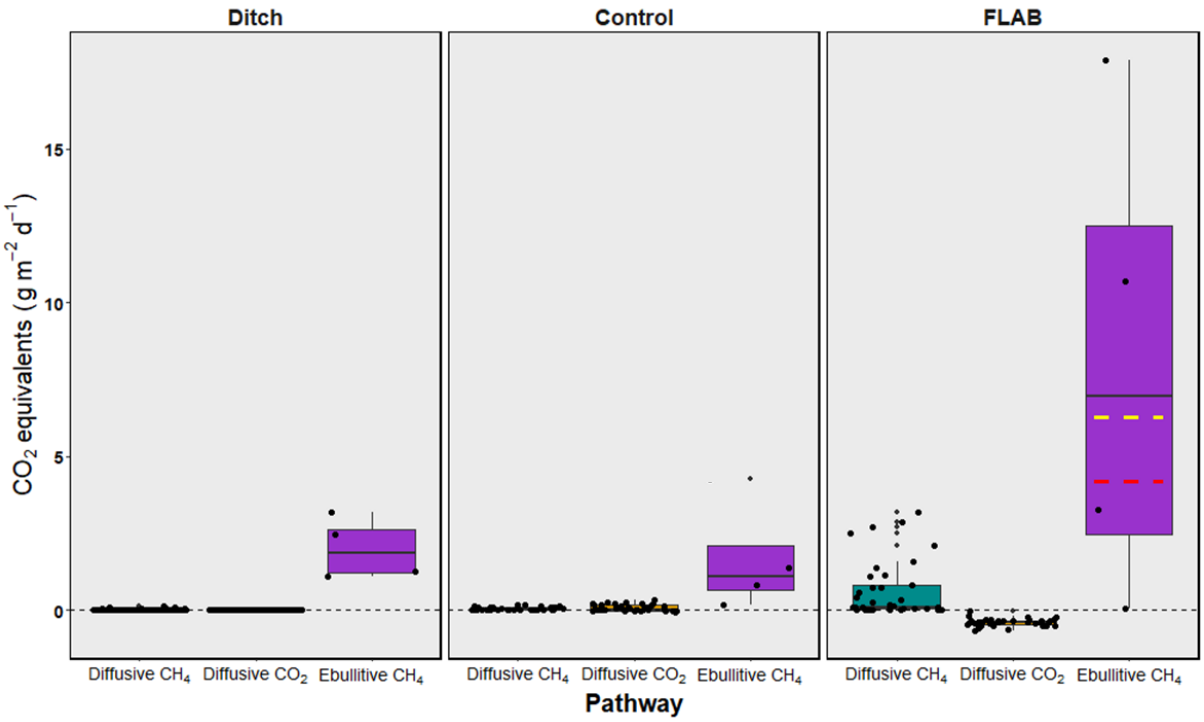

Figure 5. CO_2 equivalent emissions (g CO_{2eq} m^{-2} d^{-1}). Each panel corresponds to a different treatment (ditch, Control or FLAB treatment) and the different boxes relate to the different emissions pathways: CH_4 and CO_2 diffusive fluxes and CH_4 ebullitive emissions. In the FLAB panel, the red and yellow lines depicted on top of the ebullitive pathway boxplot correspond to the median associated with a 10% or 40% retention of ebullitive flux, correspondingly, due to the potential effect of FLAB on bubble retention.

3. Modelling CH_4 concentrations in the enclosures

Below, the results obtained for each component of the mass balance (equation 14) and the overall results are addressed separately.

3.1. *Sed*: sediment CH_4 production

Sediment CH_4 fluxes obtained from sediment cores averaged 0.5 ± 0.4 nmol CH_4 g wet weight $sediment^{-1}$ h^{-1} (range: 0.04 ± 0.00 to 1.4 ± 0.0 nmol CH_4 g wet weight $sediment^{-1}$ h^{-1}; Table S2) and were comparable between August (0.4 ± 0.2 nmol CH_4 g wet weight $sediment^{-1}$ h^{-1}) and October (0.5 ± 0.5 nmol CH_4 g wet weight $sediment^{-1}$ h^{-1}); therefore, all measurements were pooled to model sediment CH_4 production.

The mean sediment CH_4 production rates were of 0.64 ± 0.11; 0.47 ± 0.03 and 0.57 ± 0.04 nmol CH_4 gr wet weight $sediment^{-1}$ h^{-1} for the ditch, the control and the FLAB treatment, respectively, indicating no clear differences among them. Conversely, the mean sediment CH_4 oxidation rates were of 1.96 ± 0.00, 1.88 ± 0.00 and 0.86 ± 0.02 nmol CH_4 gr wet weight $sediment^{-1}$ h^{-1} for the ditch, the control and the FLAB treatment, respectively, where the

ditch and control treatment had a similar pattern whereas the FLAB treatment had a lower sediment CH_4 oxidation rate.

The mean sediment CH_4 production rates obtained from the two methods were consistent, indicating that both approaches are suitable. However, the laboratory incubations may overestimate CH_4 production and oxidation rates because the controlled conditions are optimized to favour each process. In contrast, the sediment core measurements capture a broader (and likely more realistic) range of potential *in-situ* CH_4 production. For this reason, we selected the mean, minimum, and maximum values derived from the August and October core measurements and used them as three potential scenarios of sediment CH_4 production in the model.

3.2. *MOX*: methane oxidation rates in the water

Up to 60h of incubation, both light and dark treatments had a similar pattern and no significant changes in dissolved CH_4 were detected. After this threshold, CH_4 concentration decreased in both treatments, fastest in the dark treatment (Fig. S13). This time frame after 60h was used to estimate the MOX rate of each treatment, as the slope from the regression between the dissolved CH_4 (μmol L^{-1}) and time (day), obtaining a rate of -1.3 μmol L^{-1} d^{-1} and -5.3 μmol L^{-1} d^{-1} for the light and dark treatment, respectively. Given that these rates represent either a scenario with constant light or with constant darkness, a third scenario that would include both situations was obtained as the mean rate of these two (-3.3 μmol L^{-1} d^{-1}). These three rates were used as three different potential scenarios for MOX in the mass balance.

3.3. *FLAB*: floating algae bed effects on dissolved CH_4

We did not observe substantial CH_4 production in the FLAB treatments, evidenced by a similar pattern of CH_4 dissolved concentrations between FLAB and control (Fig. S14). Although from these results it cannot be concluded that FLAB is not producing CH_4 (the rate of production could be low, and therefore not captured in the resolution of this incubation experiment), for the particular modelling exercise of this manuscript it is considered that direct production of CH_4 by FLAB is negligible.

The indirect effect of FLAB on MOX rates was considered by correcting the water MOX rates (section 9.2) for the O_2 and CH_4 concentrations below the mat, at each time point. Therefore, if the algae mat affected the concentration of O_2 and CH_4, this is reflected in the model with the corresponding changes in MOX rate.

The FLAB effect was further modelled, therefore, as an extra sediment CH_4 production due to labile organic carbon input to the sediments. For this, the input rate of OC (I, g day^{-1}) of each replicate from the FLAB treatment was obtained as the difference between the final and initial FLAB dry carbon weight (44.8% of dry weight) divided by the last 48h of experiment, which is when the CH_4 emissions spiked (Fig. 2, 3 and 4). Values of I ranged

between 26 and 45 g day^{-1} (Table S3). The rest of the parameters used to model FLAB decomposition are specified in Table 1 and Table S3.

3.4. Model selection

The normalized root mean square error (NRMSE) of the final model for the FLAB treatment ranged from 26% to 45%, indicating a moderate prediction error relative to the mean observed values and suggesting that the model captured the main patterns in the data reasonably well. For the control treatment, NRMSE values ranged from 27% to 67%, reflecting a larger relative prediction error. However, this higher error was expected given the low CH_4 concentrations in the controls, where small absolute deviations translate into large relative errors. Nevertheless, predicted values (± error) remained within the range of observed concentrations.

The parameters setting resulting in the best model fits depended on the treatment and on the replicate, indicating a considerable spatial variability. The model that best described the increase in water column CH_4 concentrations in the FLAB enclosures #5 and #6 was based on the mean sediment production scenario and the mean MOX scenario; for FLAB enclosures #1 and #8 it was based on the low sediment production scenario combined with the mean and low MOX scenarios, respectively.

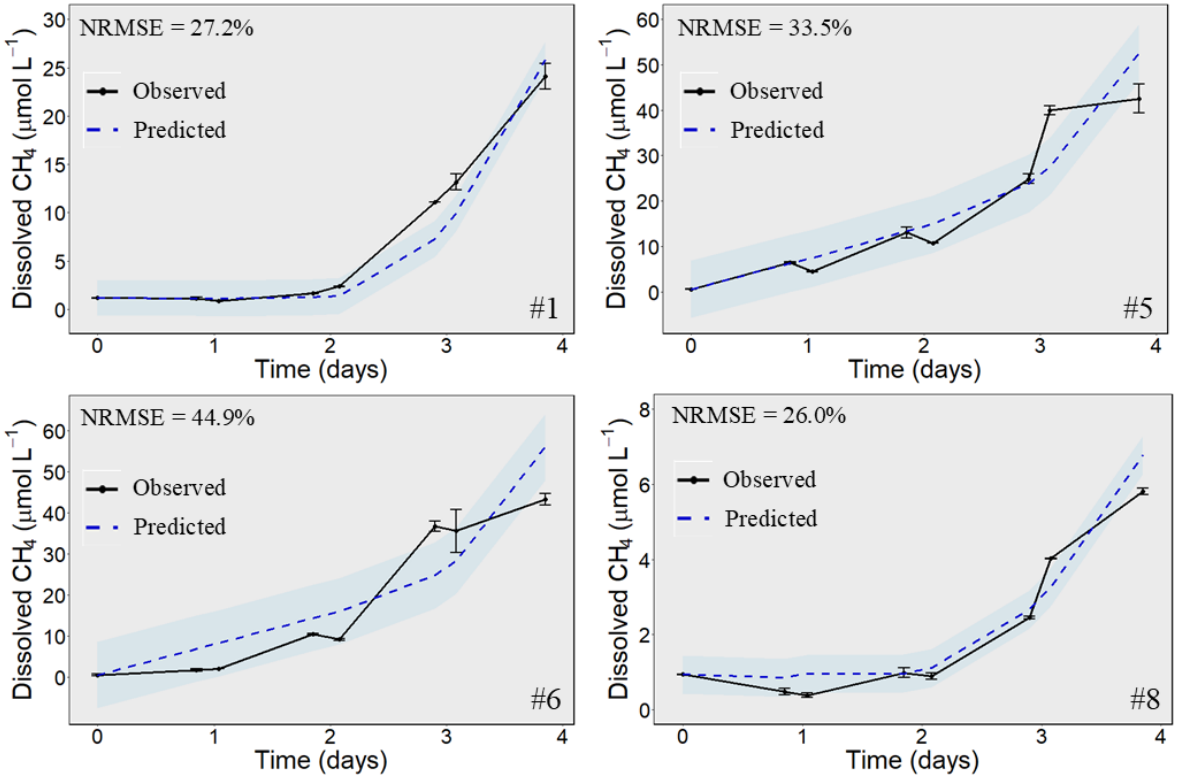

Figure 6. Modelled (blue) versus observed (black) CH_4 concentrations in each one of the four replicates of the FLAB treatment. The shaded area around the blue curve corresponds to the standard deviation of the residuals from the model. The points and error bars of the black curve correspond to the measured time points and their standard error bars.

Discussion

FLAB had a strong indirect effect on CH_4 dynamics, evidenced by higher dissolved CH_4 concentrations and substantially increased diffusive and ebullitive CH_4 emissions in the presence of floating algae, consistent with previous studies (Liang and others 2016; Grasset and others 2018). On average, CH_4 diffusive emissions were 12-fold higher and CH_4 ebullitive emissions were on average 5-fold higher in the presence of FLAB than in the control despite considerable variability among FLAB replicates. In contrast, FLAB acted as a strong daytime sink for CO_2 due to high photosynthetic activity. Although nighttime CO_2 fluxes were not measured directly, available evidence indicates that CO_2 uptake by floating primary producers during the day is often offset by nighttime respiration (Peixoto et al. 2016). Accounting for this effect did not alter the overall conclusion that FLAB substantially increased the carbon GHG total emissions of the system. The combined effects of enhanced CH_4 emissions and altered CO_2 dynamics resulted in a marked increase in CO_2-equivalent emissions in the presence of FLAB, with the overall GHG emissions being on average 4.5 times higher than that of the control, highlighting that FLAB blooms - likely to increase with nutrient enrichment and warming – play a major role in regulating carbon greenhouse gas emissions from freshwater ecosystems.

The magnitude of FLAB-induced increases in CH_4 diffusive and ebullitive emissions varied substantially among replicates, reflecting fine-scale spatial heterogeneity in sediment and water column conditions. Such variability is common in shallow freshwater systems, where differences in sediment organic matter content, redox status, and microbial activity can strongly influence baseline CH_4 production potential and the degree to which FLAB modifies local biogeochemical processes. In our experiment, replicates that developed anoxic conditions beneath the FLAB mat exhibited the largest increases in diffusive and ebullitive CH_4 emissions, consistent with the reported enhancement of methanogenesis under oxygen-depleted conditions beneath floating vegetation mats (King 1990; Kosten and others 2016). Conversely, the replicate that remained comparatively oxygenated throughout the experiment showed markedly lower dissolved CH_4 concentrations and weaker FLAB effects on both CH_4 diffusive and ebullitive fluxes. Given that all replicates received similar amount and type of FLAB, these patterns suggest that FLAB impacts on CH_4 dynamics are mediated not only by the biomass or coverage of the floating mat but also by differences in sediment properties and associated metabolic activity. Because the replicates were separated by only ~10 m in total, the observed variability underscores how small-scale heterogeneity in sediment characteristics and water–sediment interactions can modulate the strength of FLAB-driven alterations to ecosystem metabolism and GHG emissions.

The presence of FLAB also altered key physical, chemical, and biological characteristics of the ecosystem, particularly by increasing organic matter availability and reducing light and oxygen in the water column. Ash-free dry weight, DOC, TOC and turbidity in the water column were all higher in the presence of FLAB compared with both the control treatment and the ditch, consistent with previous observations of increased DOC following algal amendments (Liang and others 2016). These patterns likely arise because FLAB mats persist at the water surface while fragments remain suspended or settle, allowing them to influence the entire water column. Concomitantly, dissolved O_2 concentrations and PAR decreased under the FLAB mat, in line with findings by Pikosz and others 2017, resulting in a shift in the water column metabolism toward more heterotrophic conditions underneath the FLAB. This metabolic change is driven by shading and reduced O_2 availability beneath the floating mat, which diminishes autotrophic production, as also reported by other studies (Blindow and others 2006; Page and others 2022).

The thickness and density of the FLAB layer are key determinants of their ecological impact, with higher biomass generally associated with stronger negative effects on ecosystem functioning (Green and Fong 2016). At the start of the experiment, the wet floating biomass of FLAB averaged 20.6 ± 0.5 kg WW m^{-2}, decreasing to 4.5 ± 1.1 kg WW m^{-2} by the end of the experiment. Because the mesocosms were laterally enclosed, the biomass lost from the floating mat remained within the system, either accumulating in the water column or settling to the sediments, where it contributed to organic matter decomposition. The thickness and biomass of FLAB used in this study is comparable to that used in previous studies (Green and Fong 2016; Liang and others 2016), and resemble a natural FLAB bloom transitioning from a bloom into its decay phase, with metabolically active surface layers overlying decomposing biomass. Indeed, despite the observed decline in the mat biomass over time, all FLAB treatments remained daytime CO_2 sinks throughout the experiment (Fig. S11), indicating that active photosynthetic uptake and decomposition processes occurred simultaneously throughout the experiment.

To identify the potential mechanisms driving changes in CH_4 emissions in the presence of FLAB, a multiple approach effect was considered, including 1) potential CH_4 production directly by FLAB; 2) indirect effects on MOX rates through changes in O_2 and CH_4 dissolved below the mat; and 3) potential CH_4 production through FLAB decomposition in the sediments. There was no evidence of CH_4 production by FLAB from the laboratory incubations. Previous studies have shown that phytoplankton can produce CH_4 and rates are typically low (Klintzsch and others 2019; Bižić and others 2020; Baliña and others 2025). If FLAB were producing CH_4 at rates comparable to those reported in the studies cited above (~0.01–0.2 µmol CH_4 g^{-1} Chl-a h^{-1}) this would translate into diffusive CH_4 fluxes around 1.8 10^{-4} and 3.5 10^{-3} mg m^{-2} d^{-1} (considering the mean Chla concentration in the

FLAB treatment: 45.5 ± 30.2 μg L^{-1}, the mean enclosure volume and surface area). These rates represent less than 5% of the mean diffusive CH_4 emissions measured in the FLAB treatment, so they would not have contributed substantially to measured emissions. Regarding the indirect effect of FLAB on MOX, overall floating mats increased CH_4 and decreased O_2 concentrations beneath the mat. These changes were incorporated into the MOX calculations using a dual-substrate Monod model (Segers 1998; Guérin and Abril 2007; Martinez-Cruz and others 2015), which assumes that MOX increases with the availability of both CH_4 and O_2. Because CH_4 and O_2 were inversely related below the algae mats in our experiment, this approach may have underestimated MOX rates. Previous studies suggest that while Monod kinetics adequately describe CH_4 dependence, MOX dependence on O_2 is more complex (Rudd and others 1974; Rudd 1976) and may instead peak at high CH_4 and low O_2 concentrations (approximately 0.5 mg L^{-1}) (Thottathil and others 2019). If this relationship also applies to our system, MOX rates during the final 48 h of the experiment may have been underestimated, resulting in a conservative estimate of the indirect effect of FLAB on CH_4 dynamics. Consequently, the actual impact of FLAB on CH_4 cycling may have been greater than indicated by our MOX-corrected estimates. Nevertheless, we consider our approach appropriate because it avoids overestimating MOX activity under low-oxygen conditions.

Finally, the potential increase in CH_4 production associated with the decomposition of algal-derived organic carbon was estimated by combining parameters from our experiments and values from literature. Although such estimates are inherently uncertain, the close agreement between observed and modelled CH_4 concentrations supports the conclusion that sediment CH_4 production increased in the FLAB treatment because of enhanced decomposition of algal-derived organic matter. It is important to note that CH_4 buildup beneath FLAB likely reflects a combination of increased diffusive and ebullitive inputs (where the latter would lead to CH_4 bubble dissolution beneath the mat) which cannot be disentangled with the current dataset. Resolving these contributions would require measurements of bubble retention beneath FLAB and how trapping efficiency varies with mat thickness, as both processes are likely to play a key role in regulating FLAB-induced CH_4 emissions.

In nature, FLAB may occur as scattered patches coexisting or not with submerged macrophytes, or as dense surface blooms (Pikosz and Messyasz 2015), and these spatial differences are likely to have different effects on the total carbon emissions of the ecosystem. We emphasize that the magnitude and direction of FLAB effects depend on their spatial distribution, biomass, and interactions within the FLAB–water column–sediment continuum, which together determine the ecological conditions that develop beneath the mat. As reflected by the variability among our replicates, the effects of well-developed FLAB blooms on CH_4 dynamics can vary considerably. We attribute this variability to the extent to which the mat alters O_2 availability, as well as on intrinsic

sediment characteristics and broader climatic and limnological conditions. Consequently, the influence of FLAB on CH_4 cycling is complex, spatially heterogeneous, and temporally variable. Nonetheless, our results indicate that dense FLAB mats can substantially alter the ecological functioning and biogeochemical properties of shallow freshwater ecosystems. Our findings further support the use of FLAB as indicators of deteriorating water quality (Whitton 1984; Philips 1990; European Commission 2014; Gladyshev and Gubelit 2019), as their presence may also increase ecosystem-scale greenhouse gas emissions . As climate change is expected to promote warmer and drier conditions that favour FLAB development, positive feedback between FLAB proliferation and CH_4 emissions may emerge. This highlights the need for a better understanding of the environmental factors controlling FLAB development and persistence in freshwater systems.

References

10260 I. 1992. Water Quality – Measurement of Biochemical Parameters – Spectrometric Determination of the Chlorophyll-a Concentration. Geneva

Adair CE, Hobbie SE, Hobbie RK. 2010. Single-pool exponential decomposition models : potential pitfalls in their use in ecological studies. Ecology 91:1225–36.

Appling AP, Hall RO, Yackulic CB, Arroita M. 2018. Overcoming Equifinality: Leveraging Long Time Series for Stream Metabolism Estimation. J Geophys Res Biogeosciences 123:624–45.

Attermeyer K, Casas-Ruiz JP, Fuss T, Pastor A, Cauvy-Fraunié S, Sheath D, Nydahl AC, Doretto A, Portela AP, Doyle BC, Simov N, Gutmann Roberts C, Niedrist GH, Timoner X, Evtimova V, Barral-Fraga L, Bašić T, Audet J, Deininger A, Busst G, Fenoglio S, Catalán N, de Eyto E, Pilotto F, Mor JR, Monteiro J, Fletcher D, Noss C, Colls M, Nagler M, Liu L, Romero González-Quijano C, Romero F, Pansch N, Ledesma JLJ, Pegg J, Klaus M, Freixa A, Herrero Ortega S, Mendoza-Lera C, Bednařík A, Fonvielle JA, Gilbert PJ, Kenderov LA, Rulík M, Bodmer P. 2021. Carbon dioxide fluxes increase from day to night across European streams. Commun Earth Environ 2:1–8.

Attermeyer K, Flury S, Jayakumar R, Fiener P, Steger K, Arya V, Wilken F, Van Geldern R, Premke K. 2016. Invasive floating macrophytes reduce greenhouse gas emissions from a small tropical lake. Sci Rep 6:1–10.

Baliña S, Sánchez ML, Bizic M, Ionescu D, Thottathil SD, Bernal MC, Juárez A, Grossart H, Giorgio PA. 2025. Low contribution of oxic methane production in shallow productive lakes. :1–18.

Bižić M, Klintzsch T, Ionescu D, Hindiyeh MY, Günthel M, Muro-Pastor AM, Eckert W, Urich T, Keppler F, Grossart HP. 2020. Aquatic and terrestrial cyanobacteria produce methane. Sci Adv 6.

Blindow I, Hargeby A, Meyercordt J, Schubert H. 2006. Primary production in two shallow lakes with contrasting plant form dominance: A paradox of enrichment? Limnol Oceanogr 51:2711–21.

Borrel G, Jézéquel D, Biderre-Petit C, Morel-Desrosiers N, Morel JP, Peyret P, Fonty G, Lehours AC. 2011. Production and consumption of methane in freshwater lake ecosystems. Res Microbiol 162:832–47.

Brooks ME, Kristensen K, van Benthem KJ, Magnusson A, Berg CW, Nielsen A, Skaug HJ, Mächler M, Bolker BM. 2017. glmmTMB balances speed and flexibility among packages for zero-inflated generalized linear mixed modeling. R J 9:378–400.

Commission E. 2014. The EU Water Framework Directive. Luxembourg https://doi.org/10.2779/75229

Conrad R. 1999. Contribution of hydrogen to methane production and control of hydrogen concentrations in methanogenic soils and sediments. FEMS Microbiol Ecol 28:193–202.

Duc NT, Crill P, Bastviken D. 2010. Implications of temperature and sediment characteristics on methane formation and oxidation in lake sediments. Biogeochemistry 100:185–96.

Forney DC, Rothman DH. 2012. Inverse method for estimating respiration rates from decay time series. :3601–12.

Forster P, Storelvmo T, Armour K, Collins W, Dufresne JL, Frame D, Lunt DJ, Mauritsen T, Palmer MD, Watanabe M, Wild M, Zhang H. 2021. Climate Change 2021: the Physical Science Basis. Contribution of Working Group I to the Sixth Assessment Report of the Intergovernmental Panel on Climate Change. In: Intergovernmental Panel on Climate Change, editor. Climate Change 2021: the Physical Science Basis. Contribution of Working Group I to the Sixth Assessment Report of the Intergovernmental Panel on Climate Change. Cambridge University Press. pp 1–204.

Fuss R. 2024. gasfluxes: Greenhouse gas flux calculation from chamber measurements. CRAN (The Compr R Arch Network). https://cran.r-project.org/package=gasfluxes. Last accessed 30/12/2025

Gladyshev MI, Gubelit YI. 2019. Green Tides : New Consequences of the Eutrophication of Natural Waters (Invited Review). 12:109–25.

Gómez-Gener L, Rocher-Ros G, Battin T, Cohen MJ, Dalmagro HJ, Dinsmore KJ, Drake TW, Duvert C, Enrich-Prast A, Horgby Å, Johnson MS, Kirk L, Machado-Silva F, Marzolf NS, McDowell MJ, McDowell WH, Miettinen H, Ojala AK, Peter H, Pumpanen J, Ran L, Riveros-Iregui DA, Santos IR, Six J, Stanley EH, Wallin MB, White SA, Sponseller RA. 2021. Global carbon dioxide efflux from rivers enhanced by high nocturnal emissions. Nat Geosci 14:289–94.

Grasset C, Mendonc R, Saucedo GV, Bastviken D, Roland F, Sobek S. 2018. Large but variable methane

production in anoxic freshwater sediment upon addition of allochthonous and autochthonous organic matter. :1488–501.

Green L, Fong P. 2016. The good , the bad and the Ulva : the density dependent role of macroalgal subsidies in influencing diversity and trophic structure of an estuarine community. :988–1000.

Guérin F, Abril G. 2007. Significance of pelagic aerobic methane oxidation in the methane and carbon budget of a tropical reservoir. J Geophys Res Biogeosciences 112:1–14.

Guérin F, Abril G, Serça D, Delon C, Richard S, Delmas R, Tremblay A, Varfalvy L. 2007. Gas transfer velocities of CO2 and CH4 in a tropical reservoir and its river downstream. J Mar Syst 66:161–72.

Hall RO, Hotchkiss ER. 2017. Stream Metabolism. Elsevier Inc. http://dx.doi.org/10.1016/B978-0-12-813047-6.00012-7

Hartig F. 2023. DHARMa: Residual Diagnostics for Hierarchical (Multi-Level / Mixed) Regression Models. CRAN (The Compr R Arch Network). https://cran.r-project.org/package=DHARMa. Last accessed 30/12/2025

Hillebrand H. 1983. Development and dynamics of floating clusters of filamentous algae.

International Organization for Standardization (ISO). 1992. Water quality—Measurement of biochemical parameters—Spectrometric determination of the chlorophyll-a concentration. ISO 10260. International Organization for Standardization, Geneva, Switzerland.

Kirk JTO. 2011. Light and Photosynthesis in Aquatic Ecosystems. 3rd ed. Cambridge: Cambridge University Press

Klintzsch T, Geisinger H, Wieland A, Langer G, Nehrke G, Bizic M, Greule M, Lenhart K, Borsch C, Schroll M, Keppler F. 2023. Stable Carbon Isotope Signature of Methane Released from Phytoplankton. Geophys Res Lett.

Klintzsch T, Langer G, Nehrke G, Wieland A, Lenhart K, Keppler F. 2019. Methane production by three widespread marine phytoplankton species: Release rates, precursor compounds, and potential relevance for the environment. Biogeosciences 16:4129–44.

Klintzsch T, Langer G, Wieland A, Geisinger H, Lenhart K, Nehrke G, Keppler F. 2020. Effects of Temperature and Light on Methane Production of Widespread Marine Phytoplankton. J Geophys Res Biogeosciences 125.

KNMI. Jaar 2024 – KNMI. https://www.knmi.nl/nederland-nu/klimatologie/maand-en-seizoensoverzichten/2024/jaar?utm. Last accessed 30/12/2025

KNMI. 2026. KNMI Data Explorer. https://dataverkenner.knmi.nl/en. Last accessed 22/07/2026

Kosten S, Piñeiro M, de Goede E, de Klein J, Lamers LPM, Ettwig K. 2016. Fate of methane in aquatic systems dominated by free-floating plants. Water Res 104:200–7. http://dx.doi.org/10.1016/j.watres.2016.07.054

Lenth R. 2023. emmeans: Estimated Marginal Means, aka Least-Squares Means. CRAN (The Compr R Arch Network). https://cran.r-project.org/package=emmeans

Liang X, Zhang X, Sun Q, He C, Chen X. 2016. The role of filamentous algae Spirogyra spp . in methane production and emissions in streams. :227–39.

Liikanen ANU, Murtoniemi T, Tanskanen H. 2002. Effects of temperature and oxygen availability on greenhouse gas and nutrient dynamics in sediment of a eutrophic mid-boreal lake. :269–86.

Liu H, Zhang Q, Katul GG, Cole JJ, Chapin FS, MacIntyre S. 2016. Large CO2 effluxes at night and during synoptic weather events significantly contribute to CO2 emissions from a reservoir. Environ Res Lett 11:1–8. http://dx.doi.org/10.1088/1748-9326/11/6/064001

Magen C, Lapham LL, Pohlman JW, Marshall K, Bosman S, Casso M. 2014. OCEANOGRAPHY : METHODS A simple headspace equilibration method for measuring. :637–50.

Martinez-Cruz K, Sepulveda-Jauregui A, Walter Anthony K, Thalasso F. 2015. Geographic and seasonal variation of dissolved methane and aerobic methane oxidation in Alaskan lakes. Biogeosciences 12:4595–606.

Mendoza-lera C, Federlein LL, Knie M, Mutz M. 2016. The algal lift: Buoyancy-mediated sediment transport. Water Resour Res 52:108–18.

Nijman TPA, van Giersbergen Q, Heuts TS, Nouta R, Boonman CCF, Velthuis M, Kruijt B, Aben RCH, Fritz C. 2024. Drainage effects on carbon budgets of degraded peatlands in the north of the Netherlands. Sci Total Environ 935:172882. https://doi.org/10.1016/j.scitotenv.2024.172882

Nijman TPA, Lemmens M, Lurling M, Kosten S, Welte C, Veraart AJ. 2022. Phosphorus control and dredging decrease methane emissions from shallow lakes. Sci Total Environ 847:157584. https://doi.org/10.1016/j.scitotenv.2022.157584

Page M, Goldhammer T, Hilt S, Tolentino S, Brothers S. 2022. Filamentous Algae Blooms in a Large , Clear-Water Lake : Potential Drivers and Reduced Benthic Primary Production.

Peixoto RB, Marotta H, Bastviken D, Enrich-Prast A. 2016. Floating Aquatic Macrophytes Can Substantially Offset Open Water CO2 Emissions from Tropical Floodplain Lake Ecosystems. Ecosystems 19:724–36.

Philips DJH. 1990. Use of macroalgae and invertebrates as monitors of heavy metals in estuaries and coastal

waters. In: Furness, R. W.; Rainbow PS, editor. Heavy metals in the marine environment. Boca Raton, FL: CRC Press. pp 81–99.

Pikosz M. 2015. Oceanological and Hydrobiological Studies by.

Pikosz M, Messyasz B. 2015. Composition and seasonal changes in filamentous algae in floating mats. Oceanol Hydrobiol Stud.

Pikosz M, Messyasz B, Maciej G. 2017. Functional structure of algal mat (Cladophora glomerata) in a freshwater in western Poland. 74:1–9.

R Core Team. 2025. R: A language and environment for statistical computing. Vienna, Austria https://www.r-project.org/

RIVM. 2024. Agricultural practices and water quality in the Netherlands: status (2020–2023) and trends (1992–2023). https://www.rivm.nl/publicaties/agricultural-practices-and-water-quality-in-netherlands-status-2020-2023-and-trends

Rudd JWM. 1976. Factors controlling methane oxidation in shield lakes : The role of nitrogen fixation and oxygen concentration1. 21.

Rudd JWM, Hamilton RD, Campbell NER. 1974. John W. M. Rudd. 19:519–24.

Sander R. 2015. Compilation of Henry ' s law constants (version 4 . 0) for water as solvent. :4399–981.

Schwarz JIK, Eckert W, Conrad R. 2008. Response of the methanogenic microbial community of a profundal lake sediment (Lake Kinneret, Israel) to algal deposition. Limnol Oceanogr 53:113–21.

Segers R. 1998. Methane production and methane consumption : a review of processes underlying wetland methane fluxes. :23–51.

Simons J. 1994. Field ecology of freshwater macroalgae in pools and ditches, with special attention to eutrophication. Netherlands J Aquat Ecol 28:25–33.

Simons J, Beem AP Van. 1990. Spirogyra species and accompanying algae from pools and ditches in The Netherlands. 37:247–69.

Soued C, Prairie YT. 2021. Changing sources and processes sustaining surface CO2 and CH4 fluxes along a tropical river to reservoir system. Biogeosciences 18:1333–50.

Struik Q, Paranaíba JR, Glodowska M, Kosten S, Meulepas BMJW, Rios-Miguel AB, Jetten MSM, Lürling M, Waajen G, Nijman TPA, Veraart AJ. 2024. Fe(II)Cl 2 amendment suppresses pond methane emissions by stimulating iron-dependent anaerobic oxidation of methane.

Thottathil SD, Reis PCJ, Prairie YT. 2019. Methane oxidation kinetics in northern freshwater lakes.

Biogeochemistry 143:105–16.

Uz I, Chauhan A, Ogram A V. 2007. Cellulolytic , fermentative , and methanogenic guilds in benthic periphyton mats from the Florida Everglades.

West WE, Coloso JJ, Jones SE. 2012. Effects of algal and terrestrial carbon on methane production rates and methanogen community structure in a temperate lake sediment. Freshw Biol 57:949–55.

Westrich JT, Berner RA. 1984. The role of sedimentary organic matter in bacterial sulfate reduction : The G model tested ’. 29:236–49.

Whitman RL, Shively DA, Pawlik H, Nevers MB, Byappanahalli MN. 2003. Occurrence of Escherichia coli and Enterococci in Cladophora (Chlorophyta) in Nearshore Water and Beach Sand of Lake Michigan †. 69:4714–9.

Whitton BA. 1984. Algae as monitors of heavy metals in freshwaters. In: Shubert LE, editor. Algae as ecological indicators. London: Academic Press. pp 257–280.

Zhao P, Hammerle A, Zeeman M, Wohlfahrt G. 2018. On the calculation of daytime CO2 fluxes measured by automated closed transparent chambers. Agric For Meteorol 263:267–75. https://doi.org/10.1016/j.agrformet.2018.08.022

Supplementary information for:

Floating algal beds and methane dynamics: a potential positive feedback loop

Sofia Baliña[1], José Paranaíba[1], Maite Colina[1], Stefan Weideveld[1], Sarian Kosten[1]

[1]Ecology Department, Radboud Institute for Biological and Environmental Sciences (RIBES), Radboud University, Nijmegen, the Netherlands

Contents:

Figure S1. FLAB in Dutch drainage ditches in spring and summer in a) the province of Gelderland and b) of North Brabant, in the Netherlands.

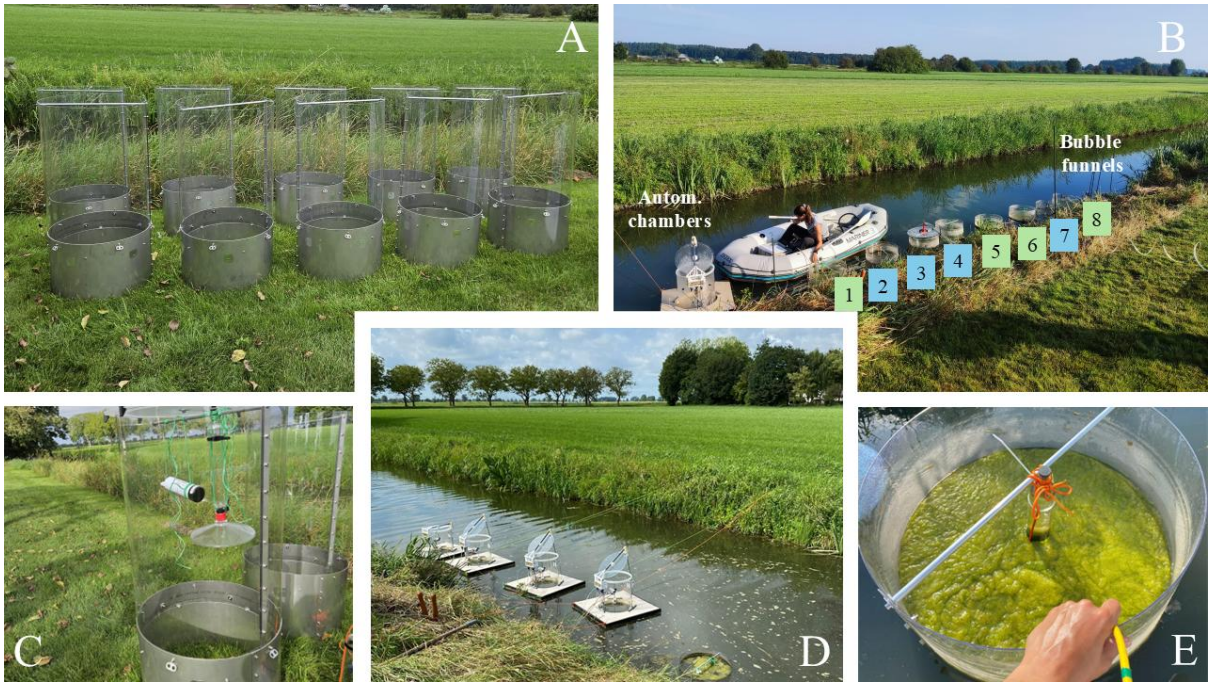

Figure S2. Set-up of field experiments. A) Enclosures just before deployment, made of transparent polycarbonate and including a stainless-steel rim in the bottom; B) General set-up of the field experiments. From upstream (i.e. upper part of the picture) to downstream: four bubble traps, the eight enclosures and the four automatic chambers. The numbers denote the eight replicates, numbers in green correspond to FLAB treatment whereas number in blue correspond to the control; C) Representation of how the high frequency sensor (miniDOT ®) and the bubble trap were placed inside of the enclosures (NOTE: the miniDOT was not placed in every enclosure, it was placed in two treatment and two control enclosures randomly selected, and another one was placed in the ditch, between the automatic chambers and the first enclosure); D) Set-up of automatic chambers, downstream the enclosures. It can be noted in the picture that one of the chambers is closed (meaning that the total CH_4 and CO_2 flux from that chamber is being measured), while the rest of the chambers are open; E) Example of an enclosure with FLAB (treatment).

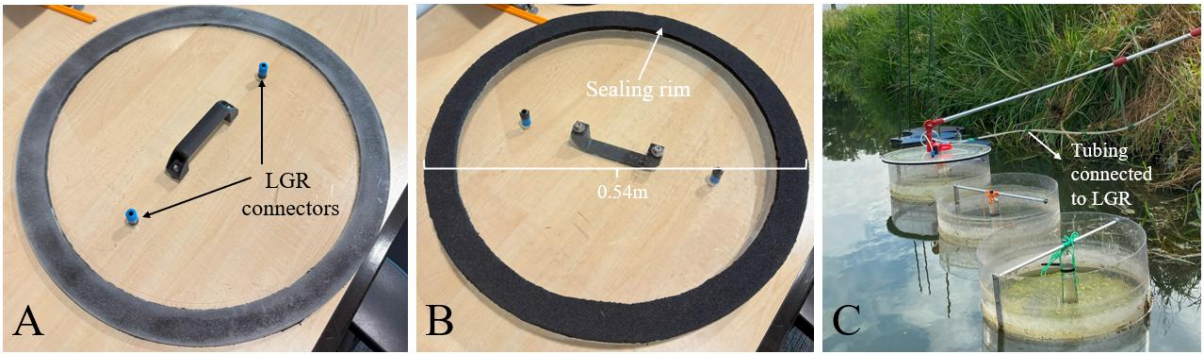

Figure S3. Lid placed on top of the enclosures to measure CH_4 and CO_2 diffusive emissions. A) Front view of the lid. LGR connectors are indicated, the tubing was connected to these ends and then to the LGR, creating a closed loop; B) Back view of the lid, where the sealing rim is in the outer section; C) Picture depicting how the lid was placed on top of the enclosures in the field.

Supplementary Information 1: Gas exchange velocity calculations

Gas exchange velocities (K) were calculated based on the obtained gas fluxes and the corresponding CH_4 concentrations in the water following equation S1 (Prairie and del Giorgio 2013; DelSontro and others 2016)

$$K = \frac{Flux\ gas}{Kh * \Delta pGas} \qquad equation\ S1$$

Where Flux gas is the diffusive flux for CH_4 (mmol m^{-2} d^{-1}), Kh is the Henry's constant correspondent corrected for atmospheric pressure and water temperature, and Δp_{Gas} is the difference between the partial pressure of the gas in the water (P_w) and the partial pressure of the gas in equilibrium with the atmosphere (P_{eq}), i.e. Δp_{Gas} (ppmv) = $P_w - P_{eq}$.

The obtained values of K were standardized to a Schmidt number of 600 (equation S2), obtaining the standardized K_{600}.

$$K_{600} = \frac{K_{CH4}}{(SC_{CCH4}/600)^{-n}} \qquad equation\ S2$$

Where Sc is the Schmidt number of a given gas at a given temperature (Wanninkhof 1992), and n is a value that depends on wind speed. A value of n = 2/3 was used for ambient wind speeds <3.7 m s^{-1} and of n = 1/2 for ambient wind speeds >3.7 m s^{-1} (Guérin and others 2007). Wind speeds were measured using a wind anemometer (Kestrel ®).

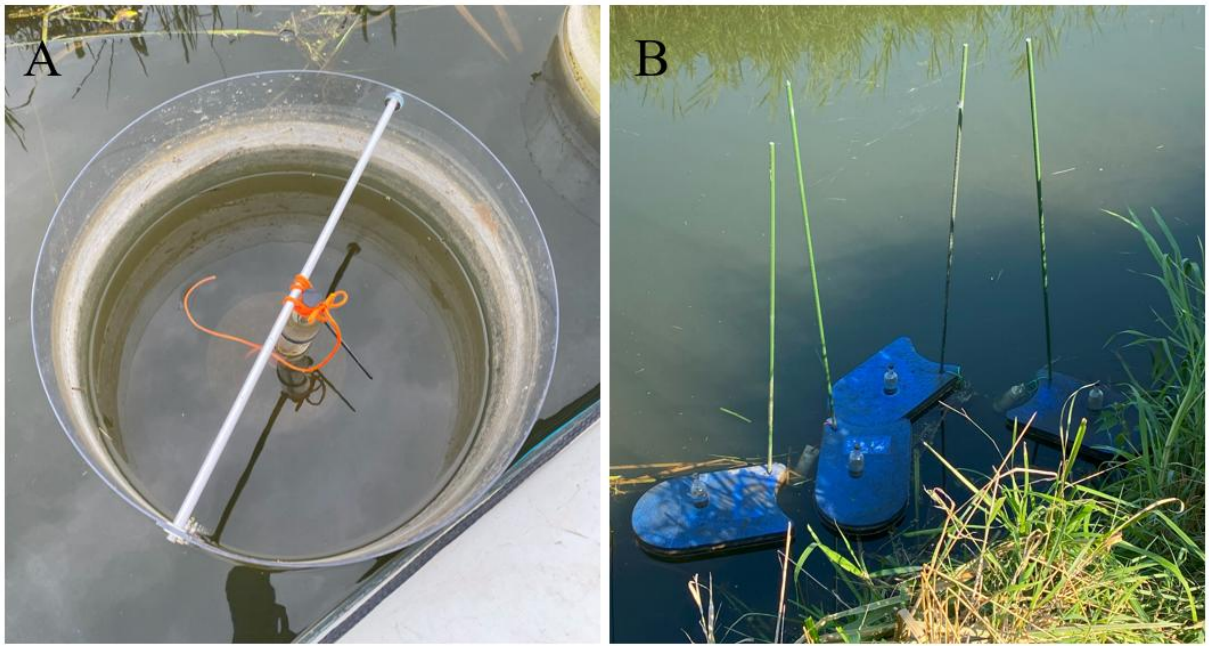

Figure S4. Pictures depicting A) how the CH_4 bubble funnels were placed in the enclosures and B) how the CH_4 bubble funnels were placed in the ditch, these last ones located upstream the enclosures.

Supplementary information 2: Assessment of water level change in the enclosures

Daily measurements of headspace height (cm) were used to calculate the change in headspace between consecutive days for each replicate. An increase in headspace indicated a loss of water from the enclosure to the ditch, whereas a decrease indicated water intrusion from the ditch into the enclosure. Using the daily headspace change (m) and the enclosure surface area (0.2 m^2), the corresponding volume change (L) was calculated and expressed as a percentage of the total enclosure volume (196.3 L). The mean absolute daily volume change across all enclosures was 4.0 ± 3.5%, ranging from 0.8% to 12.8%. Lateral water exchange was considered negligible and therefore not included in the mass balance.

Table S1. Percentage (%) of water either lost (negative) or gained (positive) in the enclosures, between consecutive days from the experimental period. There is no data from 26/8/24 to 27/8/24 because no changes were registered between these days.

Treatment	***Replicate***	***Dates***	***% of volume water either lost (negative) or gained (positive) in each replicate***
FLAB	#1	27/8/24 to 28/8/24	-11.3
		28/8/24 to 29/8/24	3.5
		29/8/24 to 30/8/24	2.0
	#5	27/8/24 to 28/8/24	-4
		28/8/24 to 29/8/24	-1.1
		29/8/24 to 30/8/24	-1.0
	#6	27/8/24 to 28/8/24	-4.6
		28/8/24 to 29/8/24	-2.2
		29/8/24 to 30/8/24	-1.0
	#8	27/8/24 to 28/8/24	5.3
		28/8/24 to 29/8/24	3.5
		29/8/24 to 30/8/24	-0.5
CONTROL	#2	27/8/24 to 28/8/24	-12.1
		28/8/24 to 29/8/24	3.5
		29/8/24 to 30/8/24	1.8
	#3	27/8/24 to 28/8/24	-12.8
		28/8/24 to 29/8/24	3.3
		29/8/24 to 30/8/24	2.4
	#4	27/8/24 to 28/8/24	-7.9
		28/8/24 to 29/8/24	-1.7
		29/8/24 to 30/8/24	1.5
	#7	27/8/24 to 28/8/24	-4.6
		28/8/24 to 29/8/24	-2.2
		29/8/24 to 30/8/24	-1.0

The tones of green correspond to replicates from the FLAB treatment, whereas the tones of blue correspond to the control treatment. The different tones in each case just provide clarity to easily identify the replicates, they do not imply any difference between them.

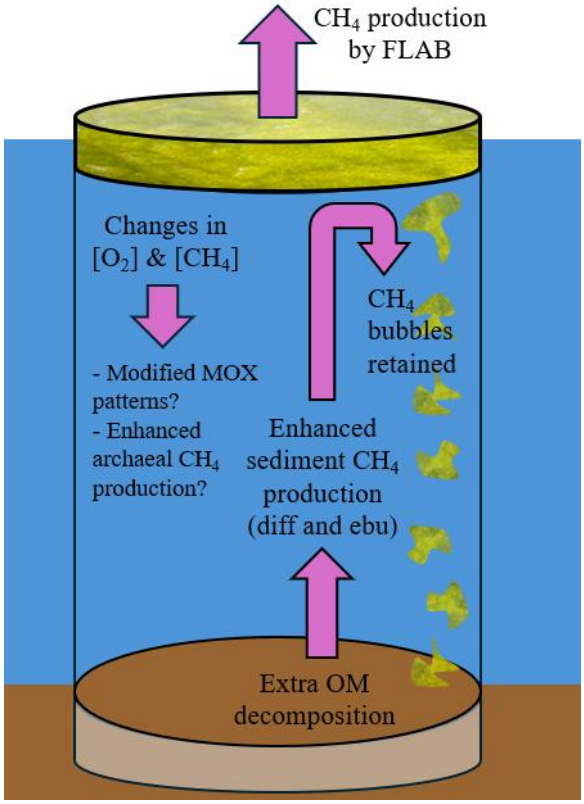

Figure S5. Schematic figure indicating the potential effects of FLAB on methane (CH_4) dynamics: FLAB could produce CH_4 directly; FLAB that sinks to the bottom can fuel extra organic matter (OM) decomposition, enhancing sediment CH_4 production, both by diffusion and/or ebullition; part of the CH_4 bubbles produced can be retained below the algae mat, increasing CH_4 dissolved concentrations below the FLAB; the algae mat can change (oxygen) O_2 and CH_4 concentration below the mat, modifying methane oxidation (MOX) patterns and/or enhancing CH_4 production by a reduction of O_2 concentrations.

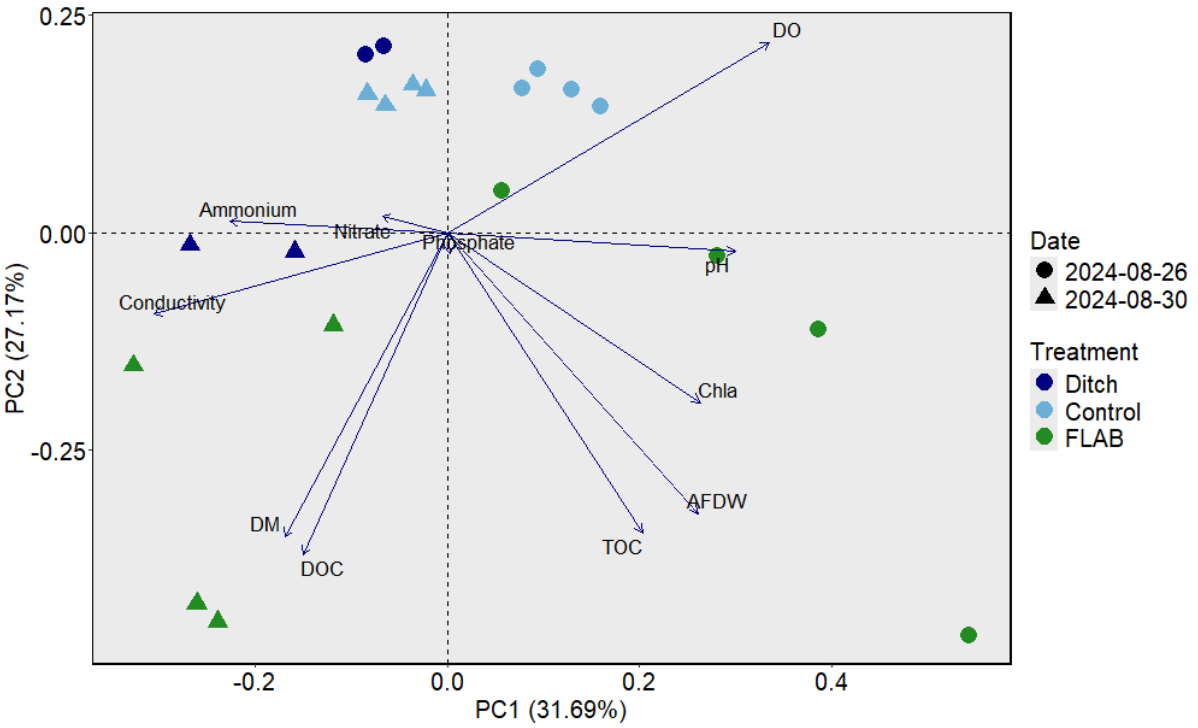

Figure S6. Biplot of principal component analysis (PCA) including data from the ditch (dark blue), from the control (light blue) and from the FLAB (green) replicates, for the onset (circles) and end (triangles) of the experimental period. The environmental variables are pH, conductivity, dissolved oxygen (DO), ammonium, phosphate, nitrate, chlorophyll a (Chla), dissolved methane (DM), dissolved organic carbon (DOC), total organic carbon (TOC), ash free dry weight (AFDW). The first principal component axis (PC1) explained 31.7% of the variation and the main variables were DO (loading = 0.44) and conductivity (loading = -0.40), which were particularly high at the onset and end of the experiment, respectively. The second principal component axis (PC2) explained 27.2% of the variation and the main variables were DOC (loading = -0.49), DM (loading = -0.46), TOC (loading = -0.45) and AFDW (loading = -0.42), all of them higher in the FLAB treatment at the end of the experiment.

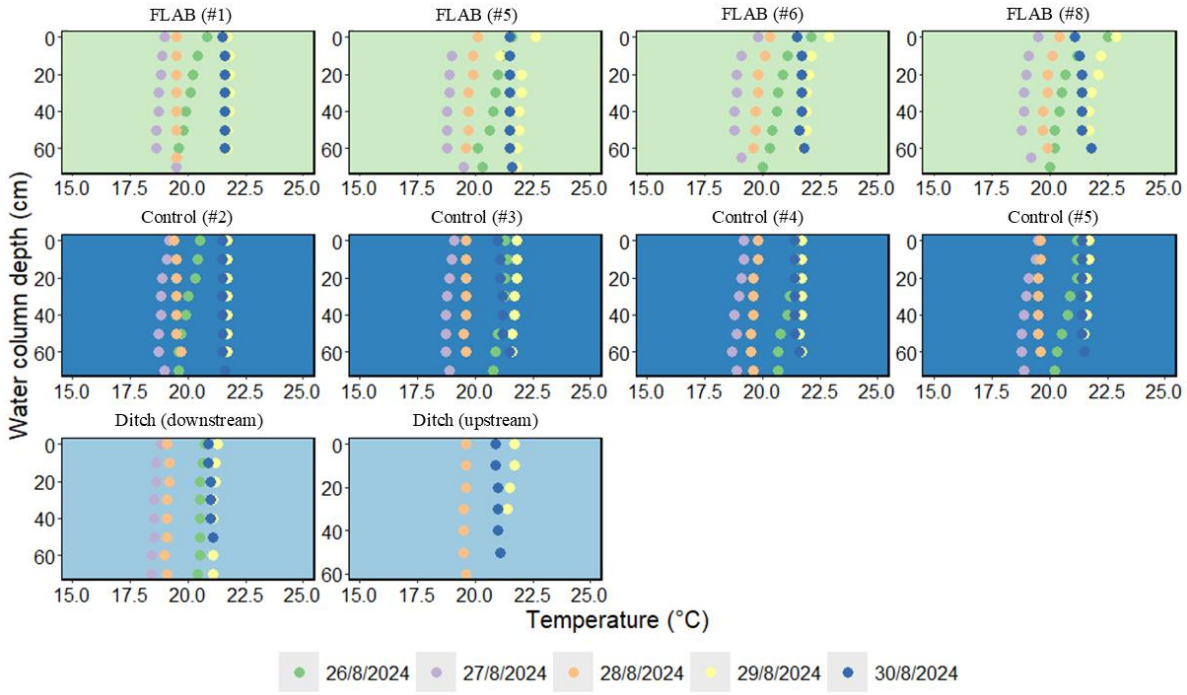

Figure S7. Daily temperature (°C) profiles carried out in the ditch (light blue), the enclosures control (dark blue) and the enclosures with FLAB (green). Each day is represented by dots with different colours. The daily profiles were carried out always in the morning, between 9am and 12hs.

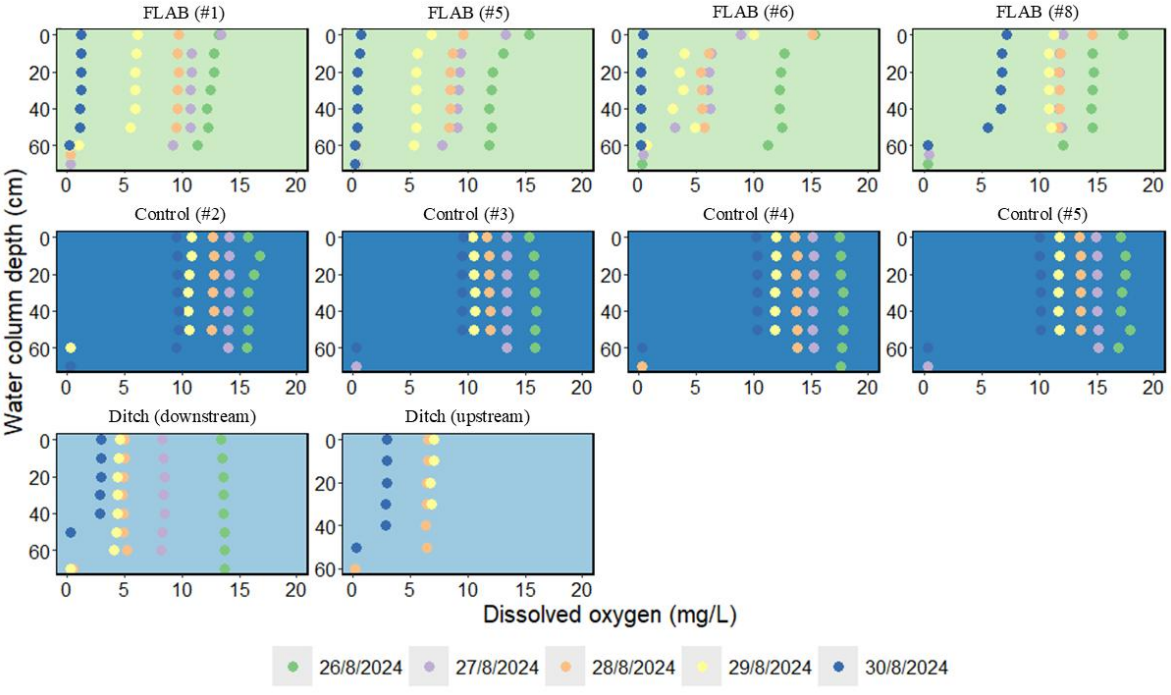

Figure S8. Daily dissolved oxygen (mg L^{-1}) profiles carried out in the ditch (light blue), the enclosures control (dark blue) and the enclosures with FLAB (green). Each day is represented by dots with different colours. The daily profiles were carried out between 9am and 12hs.

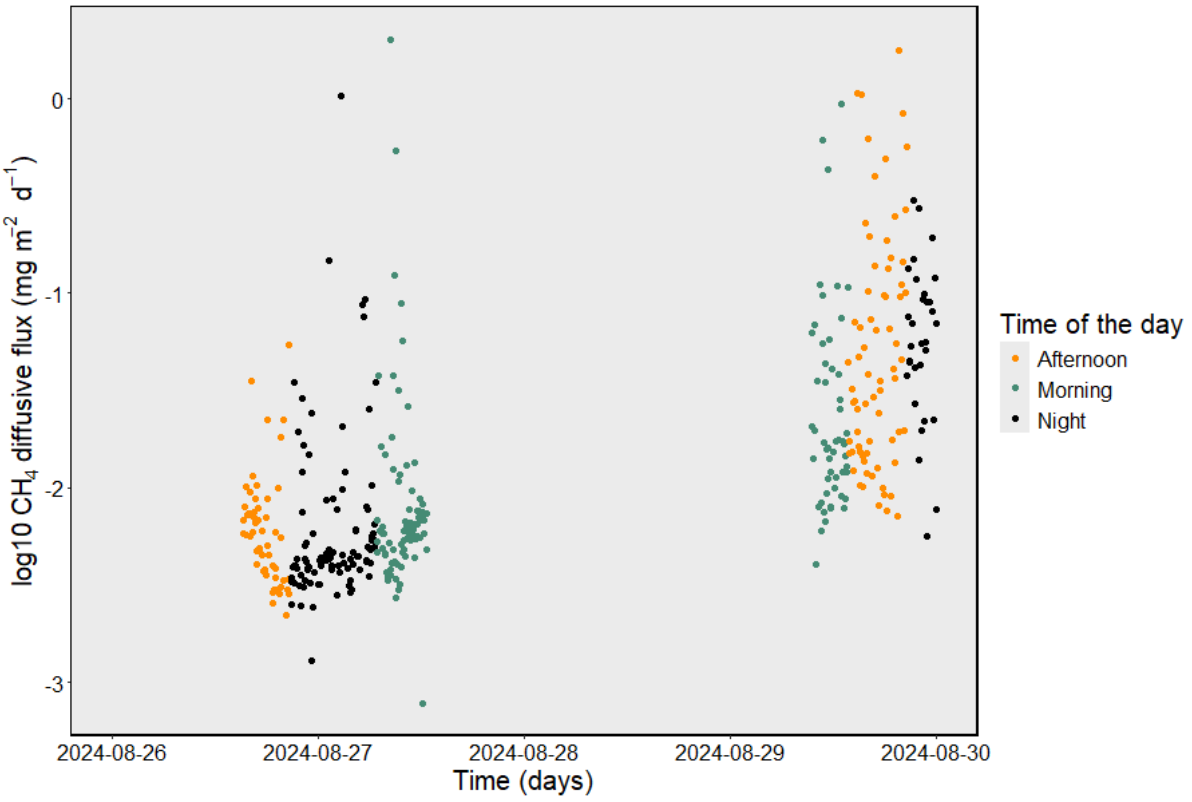

Figure S9. Log10 CH_4 diffusive emissions from the ditch, obtained with the automatic chambers. The different colours represent the moment of the day: afternoon (yellow), morning (green) or night (black). Data could be collected for the afternoon and night of the 26th of August, morning of 27th August, and also morning, afternoon and night of the 29th of August 2024.

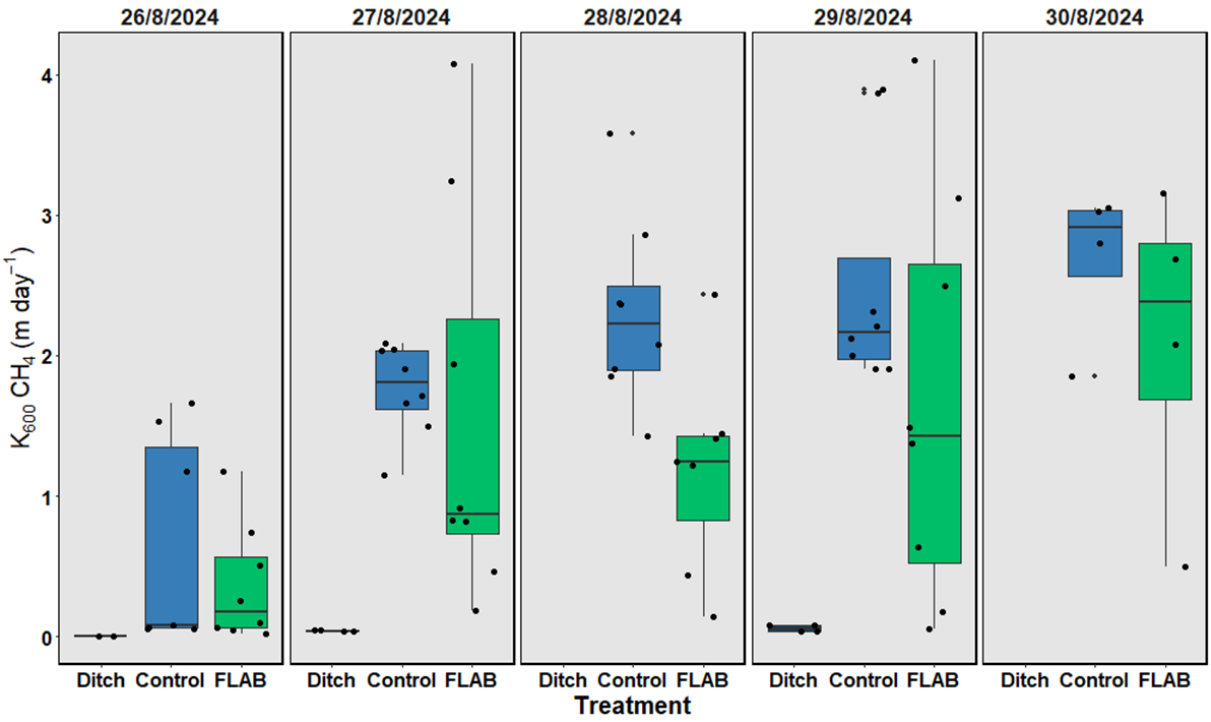

Figure S10. Methane (CH_4) standardized exchange velocities (K_{600}) for the ditch, the control and FLAB treatment. Each panel represents one day of the experimental period. For the ditch, the exchange velocity could be obtained for the same days as the CH_4 diffusive fluxes (26th, 27th and 29th of August).

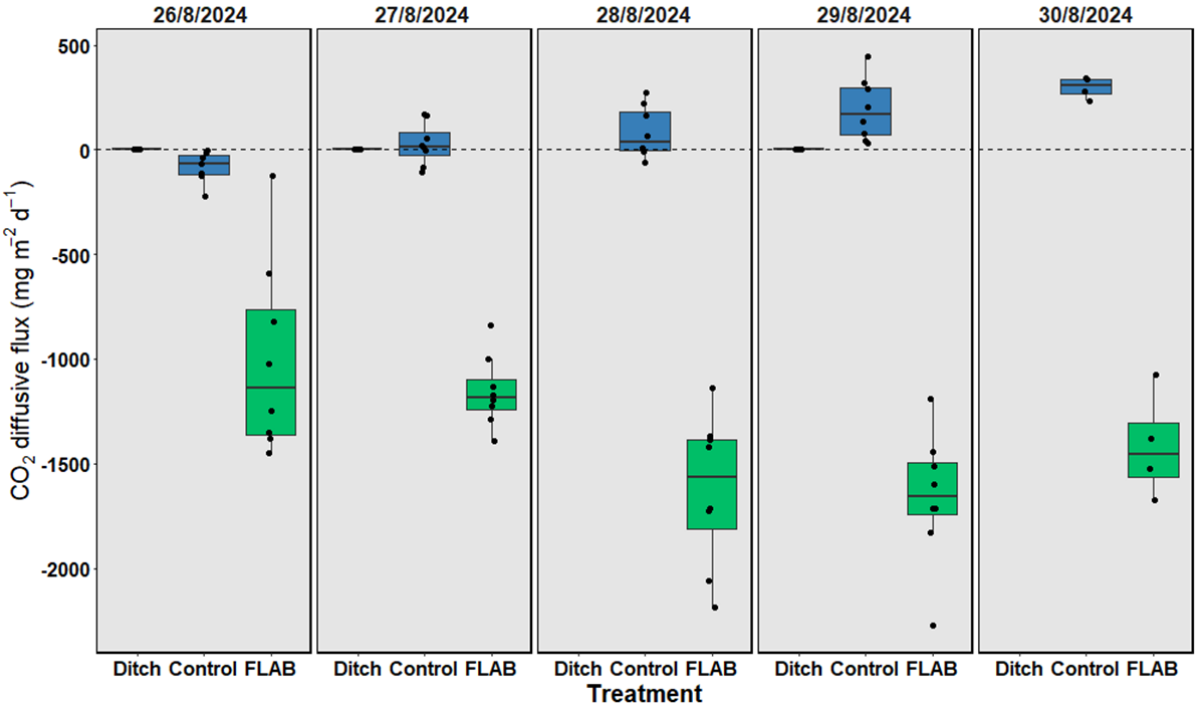

Figure S11. Carbon dioxide (CO_2) diffusive flux from the ditch, the control and FLAB treatment. Each panel represents one day of the experimental period. The dashed line represents a zero flux, higher fluxes indicate that the system is acting as a source of CO_2, whereas lower fluxes indicate that the system is acting as a sink of CO_2. Each data point from the control and FLAB treatment corresponds to a flux measured: between the 26th and the 29th two measurements were done *per* day and *per* replicate (morning and afternoon), whereas on the 30th one measurement was done *per* replicate (morning). Each data point for the ditch, corresponds to the automatically measured diffusive fluxes in the morning and/or afternoon of that day. All measurements were done during daytime.

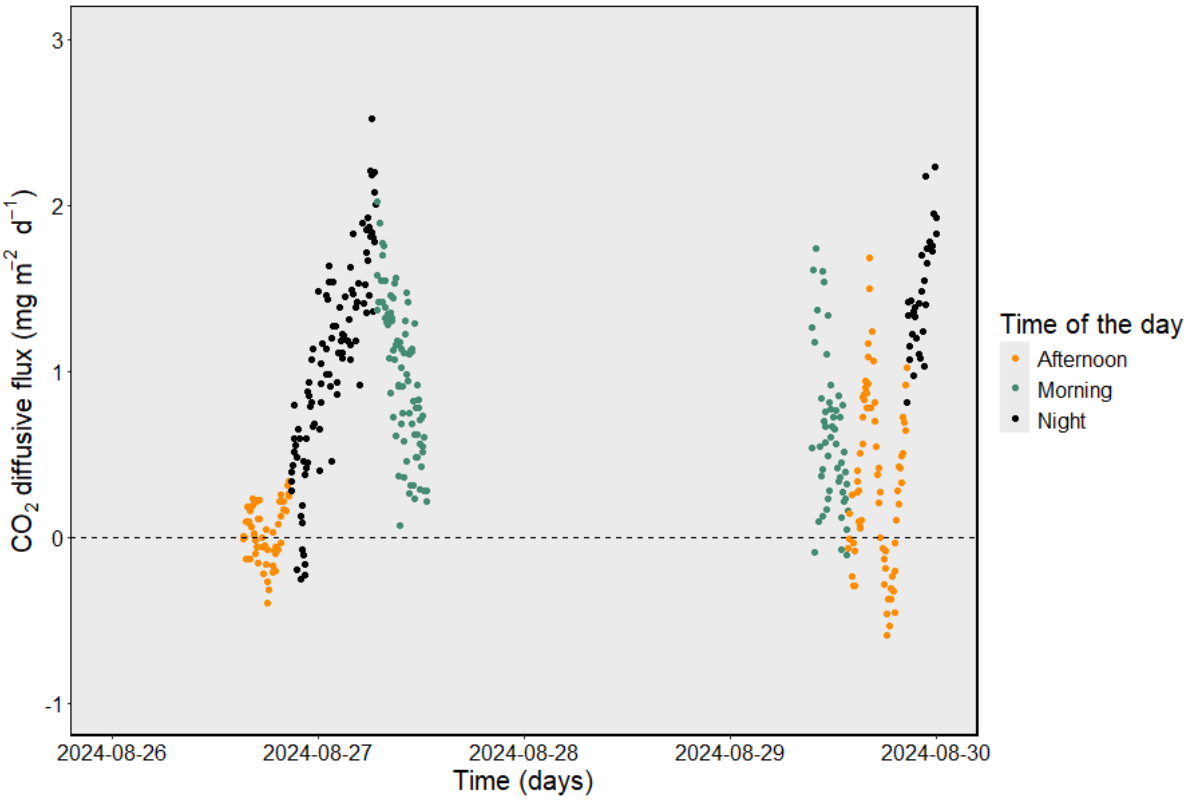

Figure S12. Carbon dioxide (CO_2) diffusive fluxes from the ditch, obtained with the automatic chambers. The different colours represent the moment of the day: afternoon (yellow), morning (green) or night (black). Data could be collected for the afternoon and night of the 26th of August, morning of 27th August, morning and afternoon of the 29th and night of the 30th of August 2024. The dashed line represents a zero flux, higher fluxes indicate that the system is acting as a source of CO_2 to the atmosphere, whereas lower fluxes indicate that the system is acting as a sink of CO_2.

Table S2: Sediment CH_4 production rates obtained from the intact core incubations and obtained from the laboratory sediment slurry incubations, as well as sediment CH_4 oxidation rates obtained from the sediment slurry incubations.

Sediment cores (n = 7)	**Ditch**		
	Min	**Mean**	**Max**
nmol CH_4 g wet weight sediment^{-1} h^{-1}	0.04	0.47 ± 0.44	1.4
Sediment incubations in laboratory	**Ditch**	**Control**	**FLAB**
CH_4 production nmol CH_4 g wet weight sediment^{-1} h^{-1}	0.64 ± 0.11	0.47 ± 0.03	0.57 ± 0.04
CH_4 oxidation nmol CH_4 g wet weight sediment^{-1} h^{-1}	-1.96 ± 0.00	-1.88 ± 0.00	-0.86 ± 0.02

For the sediment cores measured *in-situ* with an LGR, a minimum, mean ± standard deviation and maximum value from all seven measured cores was calculated. For the sediment incubations, the mean ± standard deviation of production or oxidation was calculated for the core obtained from each treatment or the ditch.

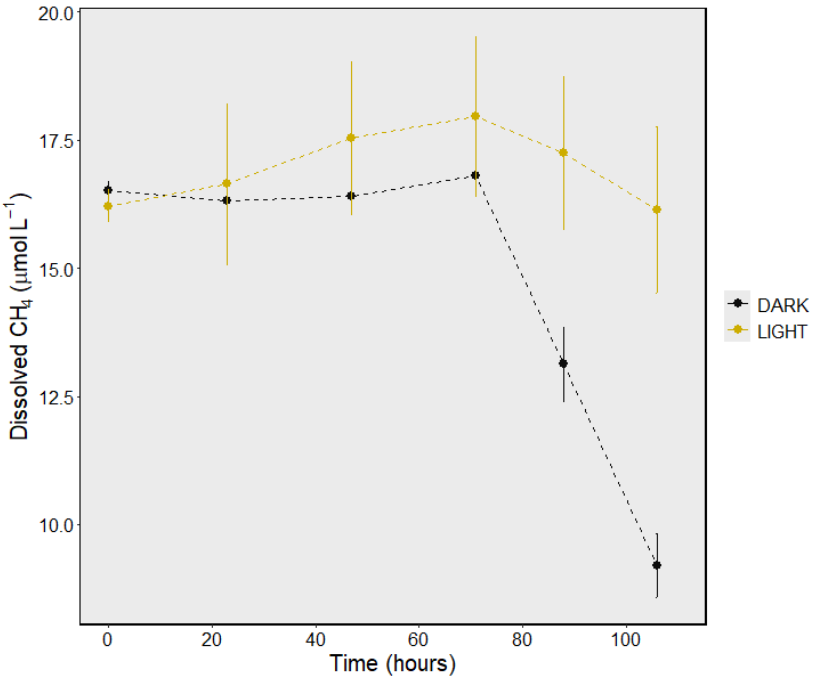

Figure S13. Incubations of water from the ditch under light (yellow) and dark (black) conditions, in all cases adding 1ml of pure CH_4 to the incubations. Data from 70h onwards was used to calculate the MOX rate for light and dark conditions, obtained as the slope of the regression between dissolved CH_4 and time. The obtained rates were -0.05 µmol L^{-1} h^{-1} (-1.3 µmol L^{-1} d^{-1}) for light conditions, and -0.2 µmol L^{-1} h^{-1} (-5.3 µmol L^{-1} d^{-1}) for dark conditions.

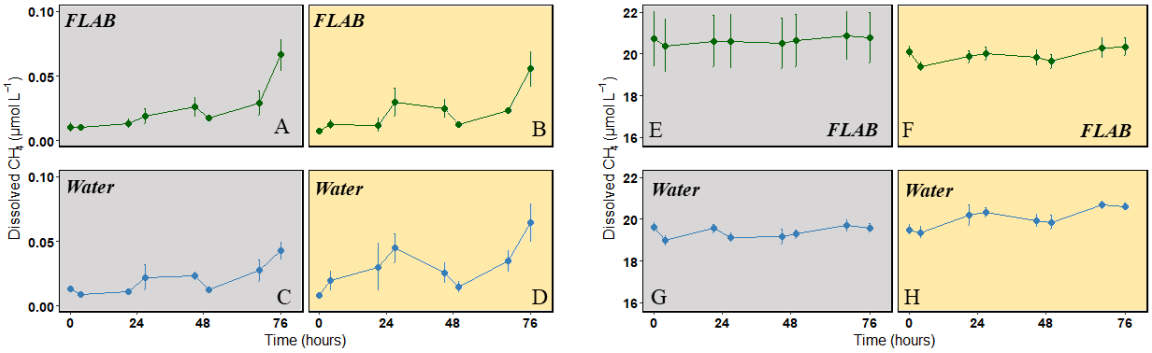

Figure S14. Incubation results for the replicates just with water (blue; C, D, G, H) of the replicates with water + FLAB (green; A, B, E, F), from the treatment under complete dark (grey) or light (yellow) conditions, and for the incubations where there was no extra addition of CH_4 (A, B, C and D) and for the incubations where CH_4 was added to the headspace (E, F, G, H). The patterns of the replicates with water or with water + FLAB do not differ in the conditions either with or without CH_4 addition.

Table S3. Scenarios selected to model FLAB effect in each one of the replicates from each treatment.

Treatment	Replicate ID	*Sed*	*MOX*	*I*	*f*	*NRMSE*
FLAB	1	Low	Low	26.7	0.04	27.2
	5	Mean	Mean	37.5	0.03	33.5
	6	Mean	Mean	45.2	0.03	44.9
	8	Low	Mean	44.4	0.01	26.0
Control	2	Low	Low	NA	NA	45.4
	3	Low	Low			39.9
	4	Low	Low			40.6
	7	Low	High			66.8

For sediment CH_4 production (*Sed*) the low, mean and maximum scenarios corresponded to 6.2, 97.8 and 323.6 mg m^{-2} d^{-1}; for methane oxidation rates (*MOX*) the low, mean and maximum scenarios corresponded to 1.3, 3.3 and 5.3 µmol L^{-1} d^{-1}; I value correspond to the input rate of OC (g day^{-1}) originating from decaying FLAB; f is the fraction of OC that is converted to CH_4 (unitless); NRMSE is the normalized root mean square error of the model fit (as a measure of how well the model explained the measured CH_4 concentrations); values of *I* and *f* for control replicates are NA because in those cases there was no FLAB.

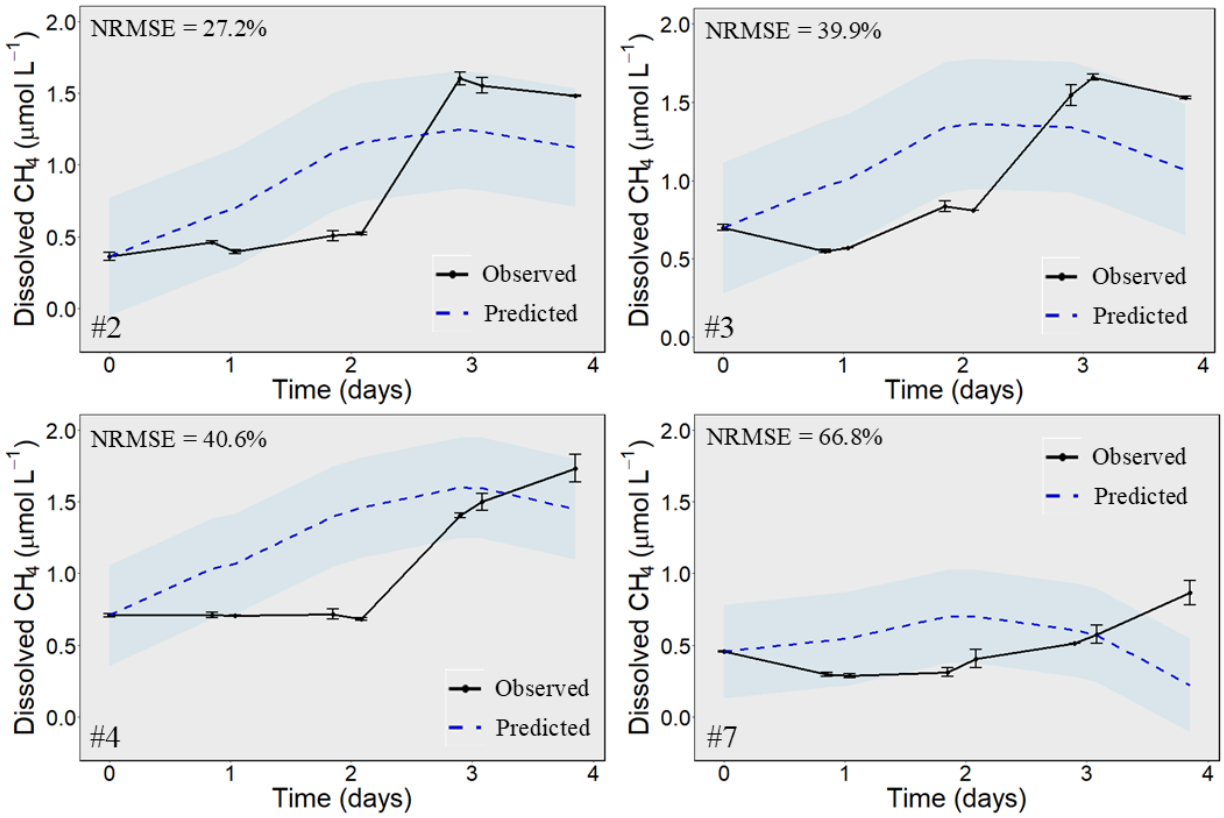

Figure S15. Modelled (blue) versus observed (black) CH_4 concentrations in each one of the four replicates of the control treatment. The shaded area around the blue curve corresponds to the standard deviation of the residuals from the model. The points and error bars of the black curve correspond to the measured time points and their standard error bars.

References

DelSontro T, Boutet L, St-Pierre A, del Giorgio PA, Prairie YT. 2016. Methane ebullition and diffusion from northern ponds and lakes regulated by the interaction between temperature and system productivity. Limnol Oceanogr 61:S62–77.

Guérin F, Abril G, Serça D, Delon C, Richard S, Delmas R, Tremblay A, Varfalvy L. 2007. Gas transfer velocities of CO2 and CH4 in a tropical reservoir and its river downstream. J Mar Syst 66:161–72.

Prairie YT, del Giorgio PA. 2013. A new pathway of freshwater methane emissions and the putative importance of microbubbles. Inl Waters 3:311–20.